Night-time oxidation of surfactants at the air–water interface: effects of chain length, head group and saturation.

Federica Sebastiani,[a,b] Richard A. Campbell,[b] Kunal Rastogi[a] and Christian Pfrang.[a*]
[a] *Department of Chemistry, University of Reading, P.O. Box 224, RG6 6AD, Reading, UK*
[b] *Institut Laue-Langevin, 71 avenue des Martyrs, CS20156, 38042 Grenoble Cedex 9, France*
* corresponding author: c.pfrang@reading.ac.uk

Abstract

Reactions of the key atmospheric night-time oxidant NO_3 with organic monolayers at the air–water interface are used as proxies for the ageing of organic-coated aqueous aerosols. The surfactant molecules chosen for this study are oleic acid (OA), palmitoleic acid (POA), methyl oleate (MO) and stearic acid (SA) to investigate the effects of chain length, head group and degree of unsaturation on the reaction kinetics and products formed. Fully and partially deuterated surfactants were studied using neutron reflectometry (NR) to determine the reaction kinetics of organic monolayers with NO_3 at the air–water interface for the first time. Kinetic modelling allowed us to determine the rate coefficients for the oxidation of OA, POA and MO monolayers to be $(2.8 \pm 0.7) \times 10^{-8}$ cm^2 molecule^{-1} s^{-1}, $(2.4 \pm 0.5) \times 10^{-8}$ cm^2 molecule^{-1} s^{-1} and $(3.3 \pm 0.6) \times 10^{-8}$ cm^2 molecule^{-1} s^{-1} for fitted initial desorption lifetimes of NO_3 at the closely packed organic monolayers, $\tau_{d,NO3,1}$, of 8.1 ± 4.0 ns, 16 ± 4.0 ns and 8.1 ± 3.0 ns, respectively. The approximately doubled desorption lifetime found in the best fit for POA compared to OA & MO is consistent with a more accessible double bond associated with the shorter alkyl chain of POA facilitating initial NO_3 attack at the double bond in a closely packed monolayer. The corresponding uptake coefficients for OA, POA and MO were found to be $(2.1 \pm 0.5) \times 10^{-3}$, $(1.7 \pm 0.3) \times 10^{-3}$ and $(2.1 \pm 0.4) \times 10^{-3}$, respectively. For the much slower NO_3-initiated oxidation of the saturated surfactant SA we estimated a loss rate of approximately $(5 \pm 1) \times 10^{-12}$ cm^2 molecule^{-1} s^{-1} which we consider to be an upper limit for the reactive loss, and estimated an uptake coefficient of ca. $(5 \pm 1) \times 10^{-7}$. Our investigations demonstrate that NO_3 will contribute substantially to the processing of unsaturated surfactants at the air–water interface during night-time given its reactivity is ca. two orders of magnitude higher than that of O_3. Furthermore, the relative contributions of NO_3 and O_3 to the oxidative losses vary massively between species that are closely related in structure: NO_3 reacts ca. 400 times faster than O_3 with the common model surfactant oleic acid, but only ca. 60 times faster with its methyl ester MO. It is therefore necessary to perform a case-by-case assessment of the relative contributions of the different degradation routes for any specific surfactant. The overall impact of NO_3 on the fate of saturated surfactants is slightly less clear given the lack of prior kinetic data for comparison, but NO_3 is likely to contribute significantly to the loss of saturated species and dominate their loss during night-time. The retention of the organic character at the air–water interface differs fundamentally between the different surfactant species: the fatty acids studied (OA and POA) form products with a yield of ~ 20% that are stable at the interface while NO_3-initiated oxidation of the methyl ester MO rapidly and effectively removes the organic character (≤ 3% surface-active products). The film-forming potential of reaction products in real aerosol is thus likely to depend on the relative proportions of saturated and unsaturated surfactants as well as the head group properties. Atmospheric lifetimes of unsaturated species are much longer than those determined with respect to their reactions at the air–water interface, so that they must be protected from oxidative attack *e.g.* by incorporation into a complex aerosol matrix or in mixed surface films with yet unexplored kinetic behaviour.

Keywords: aerosol surface, atmospheric reactions, oleic acid, palmitoleic acid, methyl oleate, stearic acid, nitrate radicals, neutron reflectometry.

1. Introduction

Over the last decades, aerosols have attracted increasing attention from the scientific community because their impact on the Earth's radiative balance and on cloud formation is still largely unknown (Shindell et al., 2009; Stevens et al., 2009; Stocker et al., 2013). Atmospheric aerosols derive from natural processes (e.g. volcanoes, wind-blown dust and sea-spray) and from human activities (e.g. combustion and cooking). A key feature for the aerosol behaviour is the presence of organic material both in the bulk and at the surface (Fuzzi et al., 2006). Organic compounds contained in atmospheric aerosols are often surface-active, such as fatty acids. Atmospheric fatty acids include saturated (such as palmitic acid; Adams & Allen, 2013) as well as unsaturated acids *e.g.* oleic acid which is found as component of marine (Tervahattu et al., 2002a; Tervahattu et al., 2002b; Fu et al., 2013) and cooking (Allan et al., 2010) aerosol. Cooking emissions have been estimated to contribute ca. 10% to the man-made emission of small particulate matter ($PM_{2.5}$) at 320 mg per person per day based on measurements in London (Ots et al., 2016). The composition and lifetime of aerosol particles in the atmosphere are largely determined by the ageing process due to exposure to trace gases, such as NO_3, OH, O_3 or other oxidants (e.g. Cl and Br; Estillore et al., 2016). To study the aerosol ageing it is crucial to investigate the heterogeneous reactions occurring between the particles and gas-phase oxidants. While homogeneous chemistry is well described at the molecular level, the study of heterogeneous reactions remains a major challenge. Field measurements suggest that heterogeneous reactions may change the chemical composition of particles and in particular of their surface films (Robinson et al., 2006). The reactions may alter important properties of the particles like aerosol hydrophilicity, toxicity and optical properties. Most of the studies to date have investigated the heterogeneous reaction of organic aerosols by O_3 and OH, which are the main oxidants during daytime. During night-time, [OH] is very low while the concentration of the photo-labile NO_3 will build up and becomes significant. Therefore while OH controls the chemistry of the daytime atmosphere, NO_3 radicals have a similar role during the night (Wayne et al., 1991; Mora-Diez et al., 2002; Ng et al., 2017). In many cases heterogeneous reactions have been studied using organic droplets or thick films (e.g. King et al., 2004; Gross et al., 2009). However, it has been shown that experimental studies of organic molecules self-assembled at the surface of water rather than purely organic aerosols alone are key to understanding atmospheric ageing of aerosols covered in organic material (Vesna et al., 2008).

In the work presented here organic monolayers at the air–water interface are used as proxies for the organic-coated aqueous atmospheric aerosols, and their reactions with NO_3 are investigated. The molecules chosen for this study are oleic acid (OA), palmitoleic acid (POA), methyl oleate (MO) and stearic acid (SA). OA (King et al., 2004; King et al., 2009; King et al., 2010), POA (Huff Hartz et al., 2007; Pfrang et al., 2011), MO (Hearn et al., 2005; Zahardis & Petrucci, 2007; Xiao & Bertram, 2011; Pfrang et al., 2014, Sebastiani et al., 2015) and SA (Sobanska et al., 2015) are popular model systems for atmospheric surfactants. MO, the methyl ester of OA, is a main component of biodiesel (chemical name: fatty acid methyl esters or 'FAME'; Wang et al., 2009) likely leading to an increased atmospheric abundance in the future since up to 7% of FAME is added to standard petroleum diesel in the EU to reduce greenhouse gas emissions; higher proportions of FAME in petroleum diesel

(10% FAME sold as 'B10' and 20% FAME sold as 'B20') as well as pure FAME ('B100') become increasingly common fuel alternatives across a number of European countries including Germany, France and Finland.

This selection of molecules allows the investigation of the effects of chain length, head group and degree of unsaturation on the reaction kinetics and products formed. The surface excess of the organic molecule during the oxidation reaction is monitored using neutron reflectometry (NR). NR is a powerful technique that can be used to determine the surface excess of a deuterated monolayers at the air–ACMW (air contrast matched water) interface (Lu et al., 2000), and information about reaction mechanisms can even be accessed thanks to partial deuteration of the surfactant (Thompson et al., 2010; Thompson et al., 2013). Further, the surface composition of mixed systems can be resolved in situ during dynamic processes by the selective deuteration of different components (Campbell et al., 2016; Ciumac et al., 2017), and therefore the reaction rates of individual components in mixtures holds great potential for future studies. In the present work, NR is used effectively to measure the surface excess of organic material (i.e. the combination of reactants and insoluble, involatile products) in situ during reactions with gas-phase NO_3.

The study of heterogeneous reactions of NO_3 at the air–water interface is made possible thanks to four recent key advances. First, the high flux and the stability of the neutron reflectometer FIGARO (Fluid Interfaces Grazing Angles ReflectOmeter, Campbell et al., 2011) at the Institut Laue-Langevin (Grenoble, France) is exploited through the acquisition of data at the air–water interface that is far faster than was previously possible (King et al., 2009; King et al., 2010). Second, surface excesses down to monolayer coverage on the order of a few percent can now be determined precisely through a refined method of background treatment (Pfrang et al., 2014). Third, improvements in the sample environment have been achieved by the design and commissioning of a new reaction chamber that has a gas delivery system optimised for homogeneous diffusion (Sebastiani et al., 2015). Lastly, rigorous measurements of the oxidant concentrations and development of a kinetic model (Pöschl et al., 2007; Shiraiwa et al., 2009; Shiraiwa et al., 2010) to interpret the data have been undertaken. Specifically, NO_3 is produced in situ by reacting O_3 with NO_2, the dependence of $[NO_3]$ on the initial $[NO_2]$ and $[O_3]$ is modelled, and to determine the concentration of NO_3, the steady state concentrations of NO_2 and N_2O_5 are measured using FTIR spectroscopy as a function of the initial $[NO_2]$.

The analysis of the kinetic experiments required the development of a modelling approach to describe all the relevant reactions and processes. In order to describe the NO_3-initiated oxidation we used a model, which considers, in addition to reactions, other mechanisms, such as accommodation, desorption, competition for adsorption sites and transport of the gas-phase species. This model builds on the formalism and terminology of the "PRA framework" (introduced by Pöschl, Rudich and Ammann in Pöschl et al., 2007). It is a combination of K2–SURF , kinetic double-layer surface model (Shiraiwa et al., 2009) and KM–SUB, kinetic multi-layer model of aerosol surface and bulk chemistry (Shiraiwa et al., 2010), but has been adapted to a planar geometry. KM–SUB and K2–SURF have been applied to describe a range of experimental datasets and conditions (e.g. Pfrang et al., 2011). Both models describe the evolution of the kinetic parameters of an organic droplet exposed to oxidants. We have adapted the model to a monomolecular organic layer at the air–water interface for analysis and interpretation of the experimental data presented here. The kinetic analysis of the measured surface excess

decays for the four reaction systems provides information on the rate coefficients of the heterogeneous reaction as well as indirect information on the formation of surface-active products. The results obtained for the different molecules will be discussed in relation of their chemical structures. Furthermore, the comparison between NO_3 and other oxidants species indicates to what extent night-time oxidation is important to atmospheric aerosol ageing. We also estimated oxidant uptake coefficients and compared those to literature data on similar organic molecules that have been studied in the condensed phase (i.e. droplets or thick films; King et al., 2004 and Gross et al., 2009).

2. Methods

2.1. Experimental

2.1.1 Materials

The organic monolayers comprised either deuterated oleic acid (d_{34}OA, $CD_3(CD_2)_7CD{=}CD(CD_2)_7CO_2D$, Sigma-Aldrich, isotopic purity ≥ 98%, purity 99%), partially deuterated palmitoleic acid (d_{14}POA, $CH_3(CH_2)_5CH{=}CH(CD_2)_7CO_2H$, custom-synthesised by the Oxford Deuteration Facility), deuterated methyl oleate (d_{33}MO, $CD_3(CD_2)_7CD{=}CD(CD_2)_7CO_2CH_3$, custom-synthesised by the Oxford Deuteration Facility, ~ 95%) and deuterated stearic acid (d_{35}SA, $CD_3(CD_2)_{16}CO_2H$, Sigma-Aldrich, isotopic purity 98%, purity 99%); further details may be found in section 1 of the ESI; the chemical structures of the molecules studied are displayed in Scheme 1. The subphase was a mixture of 8.1% by volume D_2O (Sigma Aldrich) in pure H_2O (generated using a Millipore purification unit, 18.2 MΩ cm), known as air contrast matched water (ACMW). Chloroform (Sigma-Aldrich, > 99.8%) and O_2 (Air Liquide, France, > 99.9%) were used as supplied. NO_2 was supplied in small gas cylinders (112 dm^3) by Scientific and Technical Gases Ltd (Newcastle-under-Lyme, UK) and provided as a mixture with synthetic air at a concentration of 1000 ppm with an analytical tolerance of ± 2%. The solutions of organic molecules in chloroform were prepared shortly before the experiments and the concentrations are given in mg of solute in volume of solution: for d_{34}OA 1.41 mg ml^{-1}, for d_{14}POA 1.26 mg ml^{-1}, for d_{33}MO 1.11 mg ml^{-1} and for d_{35}SA 0.58 mg ml^{-1}.

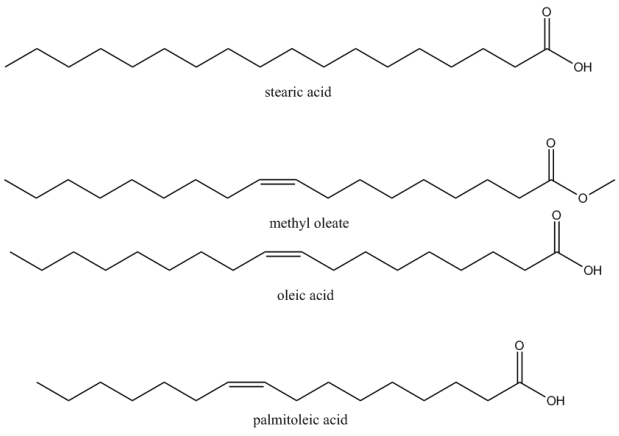

Scheme 1. Chemical structures of the organic molecules studied.

2.1.2 Gas Delivery

Nitrate radicals, NO_3, were produced *in situ* from the reaction of O_3 with NO_2. O_3 was generated by the exposure of molecular oxygen to UV light (the procedure has been described elsewhere; Pfrang et al., 2014). $[NO_3]$ was regulated by changing the flow rate of NO_2 in the range 0.045 – 0.23 $dm^3\ min^{-1}$ while $[O_3]$ was kept constant at 3.9 ppm (i.e. using a constant UV exposure of the O_2 molecules and a fixed O_2 flow rate of 1.2 $dm^3\ min^{-1}$). A flow of the NO_3-NO_2-N_2O_5-O_2 mixture was then admitted to the reaction chamber (Sebastiani et al., 2015) and the organic monolayer was oxidised at a rate that was determined by $[NO_3]$; we ensured that the reaction chamber as well as the reaction bulb where NO_2 was allowed to react with O_3 to form NO_3 was kept in the dark to avoid any photolysis of the photolabile NO_3 during the experiments. Measurements of NO_2 and N_2O_5 were carried out using IR absorption spectroscopy to establish the concentrations, $[NO_2]$ and $[N_2O_5]$, and their uncertainties. Modelling of the well-known reaction scheme allowed the estimation of $[NO_3]$. At a total flow rate of l.2 to 1.5 $dm^3\ min^{-1}$, $[NO_3]$ ranged from $(3.5 \pm 1.5) \times 10^8$ (13 ± 5 ppt) to $(2.3 \pm 1.2) \times 10^9$ molecule cm^{-3} (86 ± 45 ppt) in the experiments presented here; $[NO_3]$ and NO_2 flow rates are given in Table 1. From the gas reaction model it is found that NO_2 reaches the steady state concentration faster when initial $[NO_2]$ is higher. Ozone is consumed quantitatively in less than 250 s (see Fig. 7 in Section 3.1 of ESI). The concentration of NO_3 is lower the higher the excess of NO_2 (see Fig. 9 in Section 3.1 of ESI). The steady state concentrations of N_2O_5 are always approaching a similar value (see Fig. 8 in Section 3.1 of ESI) that is determined by the initial ozone concentration.

Table 1. The concentrations of NO_3 calculated from IR measurements of $[NO_2]$ and $[N_2O_5]$ are reported in the first column as molecule cm^{-3} and the corresponding ppt value is given in the second column; in the third column the flow rate of NO_2 is shown (the total gas mixture flow rate is obtained by adding the constant O_2 flow rate of 1.2 $dm^3\ min^{-1}$ to these values).

NO_3 / molecule cm^{-3}	NO_3 / ppt	NO_2 flow rate / $dm^3\ min^{-1}$
$(3.5 \pm 1.5) \times 10^8$	(13 ± 5)	0.360
$(4.2 \pm 1.4) \times 10^8$	(15 ± 5)	0.290
$(6.1 \pm 1.2) \times 10^8$	(23 ± 4)	0.200
$(9 \pm 3) \times 10^8$	(32 ± 10)	0.160
$(10 \pm 3) \times 10^8$	(36 ± 10)	0.130
$(9.3 \pm 2.4) \times 10^8$	(35 ± 9)	0.104
$(2.3 \pm 1.2) \times 10^9$	(86 ± 45)	0.08

The modelled concentrations were confirmed by IR measurements of $[NO_2]$ and $[N_2O_5]$ (the full dataset is displayed in Section 3.2 of ESI). Further details on the gas flow system as well as the NO_3 modelling may be found in Sections 2 and 3 of the ESI.

2.1.3 Neutron Reflectometry (NR)

NR measurements of the oxidation of deuterated monolayers by NO_3 in the reaction chamber (Sebastiani et al., 2015) were carried out on FIGARO at the Institut Laue-Langevin (Campbell et al., 2011). High flux settings were used to maximise the data acquisition rate involving an incident angle, ϑ, of 0.62°, a wavelength, λ, range of 2 – 20 Å, and a constant resolution in momentum transfer, q, of 11% over the probed q-range of 0.007 to 0.07 $Å^{-1}$, where $q = 4\pi \sin\vartheta/\lambda$.

Only a brief description of the physical basis of NR with reference to its application is given while more details may be found in Lu et al. (2000), Narayanan et al. (2017) and Braun et al. (2017). NR is a technique that can be

used to measure the surface excess of oil-like films at the air–water interface. The scattering of neutrons is related to the coherent cross sections of the atoms with which they interact, and these values vary non-monotonically with respect to different isotopes of the same atom and different atoms across the periodic table. In particular, swapping hydrogen for deuterium in molecules changes significantly the scattering, and as such mixing of hydrogenous and deuterated materials enables contrast matching.

The time-of-flight mode allowed us to follow the change in reflectivity of a deuterated monolayer at the air–water interface simultaneously over the whole measured q-range with respect to the time of the oxidation reaction. For a deuterated surfactant monolayer at the air–ACMW interface the reflectivity, R, can be expressed by:

$$R \cong \frac{16\pi^2}{q^4} 4b^2 n^2 \sin^2\left(\frac{qd}{2}\right) \quad (1)$$

where b is the scattering length of the surfactant, in fm, n is the number density, in $Å^{-3}$, d is the thickness of the layer in Å, and $bn = \rho$ is the scattering length density. The surface excess, Γ, is given by:

$$\Gamma = \frac{1}{A_{hg}} = \frac{\rho d}{b} \quad (2)$$

where A_{hg} is the area per molecule (or per head group). The surface excess for insoluble molecules corresponds to the surface concentration.

A stratified layer model was applied to the experimental data involving a single layer for the deuterated surfactant. It has been shown that in such a case and in this low q-range (< 0.07 $Å^{-1}$), the value of Γ is very insensitive to specific details of the model applied (Angus-Smyth et al. 2012). Therefore, fitting of the thickness with an arbitrary fixed value of the density or fitting of the density with an arbitrary fixed value of the thickness (each within reasonable bounds) gives equivalent results to within an added uncertainty of < 2 %. That is, only the fitted product ρd directly determines Γ, and the measurement approach deliberately desensitizes the data to structural information such as the actual layer thickness during the reaction in order to gain the requisite kinetic resolution. In our case, we chose to fit ρ while fixing d at the value obtained by fitting data recorded over a wider q-range (up to 0.25 $Å^{-1}$).

Normalisation of the reflectivity data was carried out with respect to the total reflection of an air–D_2O measurement. The sample stage was equipped with passive and active anti-vibration control. The reaction chamber was mounted on the sample stage, it was interfaced with the gas setup, and the trough was filled with 80 ml of ACMW. A given amount of solution was spread using a microlitre syringe in order to form the monolayer following the protocol use in other NR studies of atmospheric relevance (Pfrang et al. 2014; Sebastiani et al. 2015; Skoda et al. 2017; King et al. 2010; Thompson et al. 2010; King et al. 2009). The volume of solution spread was 24 µl for d_{34}OA, 23 µl for d_{14}POA, 32 µl for d_{33}MO and 35 µl for d_{35}SA. The solvent was allowed to evaporate before closing the chamber. The trough in the reaction chamber did not have barriers to compress the film and adjust the surface pressure, hence the desired surface pressure, in the range of 16 to 25 mN m^{-1} depending on the molecule, was achieved by spreading a calculated number of molecules on the water surface. Off-line tests using a surface pressure sensor confirmed that the surface pressure could be achieved reproducibly – between 2 to 7 % variation depending on the molecule – and the stability of the assembled film was assessed for 3–4 hours by monitoring the surface pressure or the reflectivity profile. From the surface excess obtained by NR the reproducibility is found to be within 1 to 9 %, depending on the molecule. The choice of

initial surface pressure and surface excess was based on the requirement of maximising the signal-to-noise ratio for NR measurements while having a reaction that lasts long enough to be analysed for kinetics parameters. A reduction of the initial surface pressure is not expected to affect the kinetic behaviour, i.e. the $\Gamma(t)$ will start from a lower value and the curve will extend on a shorter time and less data will be available for the kinetic fitting. An increase of spread molecules will produce more droplets floating on top of a monolayer, when the molecule is unsaturated (compare to Figures 1–3 in Section 1 of ESI), while it will introduce inhomogeneity in the monolayer formed by saturated molecule (see Fig. 4 Section 1 of ESI) preventing a reliable interpretation of the NR measurement. The monolayer was further characterised with compression-expansion isotherms with a Langmuir trough off-line, while recording Brewster-angle microscopy (BAM) images at different surface pressure values, and these results are shown in the ESI Section 1. Data were recorded for a few minutes before NO_3 was admitted into the chamber. The time resolution was 2 s. The alignment of the interface was maintained to a precision of 5 μm using an optical sensor (LK-G152, Keyence, Japan; laser class II, wavelength 650 nm, power output 0.95 mW, spot diameter 120 μm), which operated through the laser alignment window of the reaction chamber (Sebastiani et al., 2015).

2.2. Kinetic modelling

Oxidation of organic compounds by NO_3 may proceed via several reaction channels: rapid addition to the double bond of unsaturated species as well as slower abstraction of hydrogen atoms particularly relevant for saturated compounds (Wayne et al., 1991). These mechanisms as well as transport processes need to be considered in order to fit our experimental data. Based on the PRA-framework (Pöschl et al., 2007; Shiraiwa et al., 2009; Shiraiwa et al., 2010; Pfrang et al., 2010; Shiraiwa et al., 2012a), a specific model has been developed for the heterogeneous reaction of a monomolecular organic layer at the air–water interface. The oxidant loss due to the reaction and transport to the bulk water has been taken into account. The organic reactants used in the experiments show a very low solubility and slow diffusion in water, hence the loss due to transport to the bulk could be neglected. The product branching ratios of the heterogeneous reactions are not known, and we were not able to identify individual product compounds from a monomolecular film at the air–water interface. The products were thus divided into three categories: volatile, soluble and surface-active species. The distinction between soluble and volatile species is made on the basis of the product yields reported previously (Hung et al., 2005; Docherty & Ziemann, 2006) for bulk reaction and considering vapour pressures (Compernolle et al., 2011) and solubilities (Kuhne et al., 1995) of the products. In the model, the branching ratios for volatile and soluble products are based on literature values, and for surface-active products an estimation was based on $\Gamma(t)$ at long reaction times; the technique used in this study monitors the deuterium concentration at the interface, no other information can be obtained. We could have described the reaction system by assuming only two types of products: surface active and non-surface active. However, we decided to distinguish non-surface active compounds between volatile and soluble products in order to make our model suitable for description of experimental data probing the partitioning to subphase and/or gas-phase. Because of the method used to produce NO_3 (see Section 2.1.2 and Sections 2–3 of ESI) the ratio $[NO_2]/[NO_3]$ increases from 10^5 to 10^7 as $[NO_3]$ decreases from 10^9 to 10^8 molecule cm^{-3}. Since NO_2 can adsorb and desorb from the organic layer (compare King et al., 2010), occupying reactive sites for an average time represented by the desorption lifetime, the loss of organic material due to reaction with NO_3 may also be affected. The NO_2 occupies a reactive site, which

becomes unavailable for NO_3 oxidation, and hence reduces the number of reactive sites available and slows down the apparent reaction rate. In particular, for high $[NO_2]/[NO_3]$ ratios the reactant loss rate will be lower than the loss rate recorded for the lower $[NO_2]/[NO_3]$ ratios. To take this effect into account we included the absorption and desorption of NO_2 in the model and to describe it we introduced the parameter called desorption lifetime, $\tau_{d,NO2}$, following the approach used by Shiraiwa et al. (2009). The effect of N_2O_5 is not considered in the model, since the concentration was constant for all gas conditions, as shown in Figure 8 of the ESI. Experimental studies of reactive uptakes of NO_3 and N_2O_5 (Gross & Bertram, 2008; Zhang et al., 2014a; Gržinic, et al., 2015) have shown that NO_3 uptake is substantially faster with a comparative study for OA reporting a ca. four orders of magnitude higher uptake coefficient of NO_3 compared to N_2O_5 (Gross et al., 2009). The system has been modelled as a gas phase (g) and a near-surface gas phase (gs), above a sorption layer (s), a surface layer (ss), a near-surface bulk (nb) and the bulk (b), following the formalism of Shiraiwa et al. (2010) (as illustrated in Figure 1). Different to the model presented by Shiraiwa et al. (2010) we had to remove the curvature terms from the modelling code to be able to describe the flat air–water interface present in our experimental system. We do not expect any significant impact of curvature on the processes studied here.

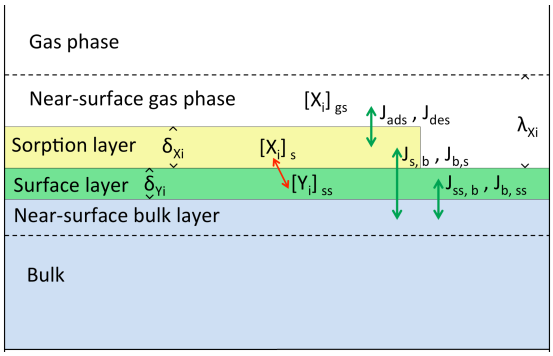

Figure 1. Kinetic model for an organic layer at the air–water interface, δ_{Xi} and δ_{Yi} are the thicknesses of sorption and surface layer. λ_{Xi} is the mean free path of X_i in the gas phase. The red arrow shows chemical reactions. The green arrows show the transport fluxes.

The gas-phase species, NO_3 and NO_2, can adsorb to the sorption layer and interact with the organic molecules in the surface layer. The products can stay at the surface layer, or they can be lost through solubilisation into the bulk or by evaporation into the gas phase.

The evolution of the gas species surface concentration, $[X_i]_s$, can be described by taking into account the following processes: adsorption, desorption, transport and reaction. Full details are given in the ESI. In the following section, only the key equations that describe the reactions are discussed (the nomenclature used is based on the PRA framework; Pöschl et al., 2007; Shiraiwa et al., 2009; Shiraiwa et al., 2010; Pfrang et al., 2010; Shiraiwa et al., 2012a).

Our gas-phase species NO_3 reacts with the organic layer and the loss, $L_{surf,Y,NO3}$, can be described with the second–order rate coefficient $k_{surf,Y,NO3}$:

$$L_{\mathrm{surf,Y,NO_3}} = k_{\mathrm{surf,Y,NO_3}} [\mathrm{Y}]_{\mathrm{SS}} [\mathrm{NO_3}]_{\mathrm{S}} \quad (3)$$

The evolution of the NO_3 surface and bulk concentrations can be described as follows:

$$\frac{d[\mathrm{NO_3}]_S}{dt} = J_{\mathrm{ads,\,NO_3}} - J_{\mathrm{des,\,NO_3}} - L_{\mathrm{surf,Y,NO_3}} + J_{\mathrm{bs,\,NO_3}} - J_{\mathrm{sb,\,NO_3}} \quad (4)$$

$$\frac{d[\mathrm{NO_3}]_b}{dt} = \left(J_{\mathrm{sb,NO_3}} - J_{\mathrm{bs,NO_3}}\right)\frac{A}{V} \quad (5)$$

where A is the water surface area and V is the total water volume. In the case of NO_2 the corresponding equation 4 does not have the L_{surf} term, since it is not reactive toward the organic molecules considered (King et al. 2010), Eq. 5 is the same. The flux of adsorbed gas molecules, $J_{\mathrm{ads,\,NO_3}}$, is proportional to the surface accommodation coefficient, $\alpha_{s,NO3}$, is determined by the product of the surface accommodation coefficient on an adsorbate–free surface, $\alpha_{s,0,NO3}$, and the sorption layer coverage θ_s which is given by the sum of the surface coverage of all competing adsorbate species (see details in Section 4.1 of ESI). The flux of desorption, $J_{\mathrm{des,\,NO_3}}$, is proportional to the inverse of the desorption lifetime, $\tau^{-1}_{\mathrm{d,\,NO_3,eff}}$, which is the average time that the NO_3 molecule occupies an adsorption site. $\tau^{-1}_{\mathrm{d,\,NO_3,eff}}$ is a combination of two desorption lifetimes, depending on the organic molecule packing at the interface, $\theta_{ss} = [\mathrm{Y}]_{ss}(t)/[\mathrm{Y}]_{ss}(0)$; either closely packed ($\tau^{-1}_{\mathrm{d,\,NO_3,1}}$), or in the gas-like state ($\tau^{-1}_{\mathrm{d,\,NO_3,2}}$):

$$J_{\mathrm{des,\,NO_3}} = k_{\mathrm{d,NO_3}}[\mathrm{NO_3}]_s = \tau^{-1}_{\mathrm{d,\,NO_3,eff}}[\mathrm{NO_3}]_s \quad (6)$$

$$\tau^{-1}_{\mathrm{d,\,NO_3,eff}} = \theta_{ss}\tau^{-1}_{\mathrm{d,\,NO_3,1}} + (1-\theta_{ss})\tau^{-1}_{\mathrm{d,\,NO_3,2}} \quad (7)$$

The organic reactant, Y, (e.g. oleic acid) can be lost just through reaction with NO_3 at the surface, hence it is described as:

$$\frac{d[\mathrm{Y}]_{ss}}{dt} = -k_{\mathrm{surf,Y,NO_3}}\,[\mathrm{Y}]_{\mathrm{SS}}\,[\mathrm{NO_3}]_{\mathrm{S}} \quad (8)$$

The products (Z) of the heterogeneous reaction cannot be identified individually at the air–water interface by the experimental techniques used, hence we divided them in three main categories: surface-active (i.e. remaining at the surface and directly measurable by NR, Z_S), volatile (i.e. escaping into the gas-phase, Z_G) and soluble (i.e. accumulating the droplet bulk, Z_B) species. Since the surface-active products (Z_S) will remain at the air–water interface, the surface–bulk transport is neglected:

$$\frac{d[\mathrm{Z_S}]_{ss}}{dt} = c_S k_{\mathrm{surf,Y,NO_3}}\,[\mathrm{Y}]_{\mathrm{SS}}\,[\mathrm{NO_3}]_{\mathrm{S}} \quad (9)$$

where c_S is the branching ratio for the surface-active products. The volatile products (Z_G) will leave the surface depending on their vapour pressures, but with a lack of information on the chemical composition, we decided to use a first-order loss rate coefficient, $k_{\mathrm{loss,G}}$, to describe the overall effect, hence the differential equation for Z_G is:

$$\frac{d[\mathrm{Z_G}]_{ss}}{dt} = c_G k_{\mathrm{surf,Y,NO_3}}\,[\mathrm{Y}]_{\mathrm{SS}}\,[\mathrm{NO_3}]_{\mathrm{S}} - k_{loss,G}[\mathrm{Z_G}]_{ss} \quad (10)$$

where c_G is the branching ratio relative to the volatile products. The bulk–surface transport is not considered for the volatile products because it is assumed to be negligible compared to the volatilisation process. The soluble products (Z_B), once formed, will diffuse into the water bulk depending on the diffusion coefficient, $D_{b,B}$, and the transport velocity can be estimated as $k_{bss,B} \approx 4\,D_{b,B}/\pi\delta_B$, where δ_B is the effective molecular diameter of the soluble species. The inverse process is described by a surface–bulk transport velocity $k_{ssb,B} \approx k_{bss,B}/\delta_B$, hence the evolution of the soluble product concentration in surface layer (ss) and bulk (b) is expressed as:

$$\frac{d[\mathrm{Z_B}]_{ss}}{dt} = c_B k_{\mathrm{surf,Y,NO_3}} [\mathrm{Y}]_{\mathrm{SS}} [\mathrm{NO_3}]_{\mathrm{S}} + k_{\mathrm{bss,B}}[\mathrm{Z_B}]_b - k_{\mathrm{ssb,B}}[\mathrm{Z_B}]_{ss} \quad (11)$$

$$\frac{d[\mathrm{Z_B}]_b}{dt} = \left(k_{\mathrm{ssb,B}}[\mathrm{Z_B}]_{ss} - k_{\mathrm{bss,B}}[\mathrm{Z_B}]_b\right)\frac{A}{V} \quad (12)$$

where c_{B} is the branching ratio for the soluble products. The equations (4)–(12) describe the evolution of the various species. This system of equations cannot be solved analytically, hence the ODE solver of MATLAB (2011) has been used for numeric solving. In order to fit $\Gamma(t)$, provided by NR, a minimisation of the value of χ^2 has been performed using the FMINUIT package (Allodi).

The product branching ratios affect the whole $\Gamma(t)$, varying c_S the final value of $\Gamma(t)$ changes, i.e. a higher c_S leads to a higher final value of $\Gamma(t)$; the model is less sensitive to changes in c_G and c_B, however change in the solubilisation and/or volatilisation kinetic parameters ($D_{\mathrm{b,B}}$ and $k_{\mathrm{loss,G}}$) will affect the decay of $\Gamma(t)$. These parameters were chosen in order to best describe the experimental data and taking into account literature data.

The kinetic model described above depends on several parameters, and some of them are strongly correlated. For example, for a given gas species time evolution, which may be described by certain accommodation coefficients ($\alpha_{\mathrm{s,0,X}i}$ where X_i is NO_3 or NO_2) and certain desorption lifetimes ($\tau_{\mathrm{d,\,X}i}$), a good fit may be obtained as well with a lower $\alpha_{\mathrm{s,0,X}i}$ combined with a higher $\tau_{\mathrm{d,X}i}$. The accommodation coefficient represents the probability of the gas-phase molecule to absorb at the organic layer, hence the lower $\alpha_{\mathrm{s,0,NO3}}$ is, the smaller is the probability of the reaction with the organic molecule. The desorption lifetime represents the mean residence time of the molecule absorbed at the surface, hence the longer this time, the higher is the probability for the gas molecule to react (valid for NO_3). NO_2 does not react with the organic layer (King et al. 2010), but those parameters still compensate, because $\alpha_{\mathrm{s,0,NO2}}$ determines the number of molecules absorbed and $\tau_{\mathrm{d,NO2}}$ determines the number of molecules leaving the sorption sites. The choice of leaving both of these parameters free to vary in the fitting will lead to a wide range of values for both. The resulting surface excess will match the experimental data. However, the choice of fixing one out of these two parameters makes the optimisation of the model computationally easier and the comparison between different organic molecules possible. In the fitting we have fixed the $\alpha_{\mathrm{s,0,X}i}$ to one for both gas species.

The desorption lifetime for the reactive species, NO_3, shows a correlation to the reaction rate coefficient, $k_{\mathrm{surf,Y,NO_3}}$, for example if the rate coefficient is kept constant an increase in desorption lifetime will lead to higher loss rate, and vice versa, if $\tau_{\mathrm{d,\,NO_3,eff}}$ is kept constant and $k_{\mathrm{surf,Y,NO_3}}$ increases the loss rate will augment. Our measurement follows the loss rate, the values for $k_{\mathrm{surf,Y,NO_3}}$ and $\tau_{\mathrm{d,\,NO_3,eff}}$ are obtained from the best fit of the model to the data.

3. Results

Three of the organic molecules considered in this work (OA, POA and MO) contain one unsaturated C=C bond in the aliphatic tail while one molecule (SA) is fully saturated. Among the unsaturated surfactants, POA has a shorter tail than OA and MO, whereas MO is a methyl ester in comparison with the fatty acids OA and POA. The double bond is expected to be the key reactive site for NO_3. Kinetic data on the three reactive unsaturated surfactants are presented first in Sections 3.1 to 3.3, respectively. Furthermore, in a separate process NO_3 is known to abstract hydrogen atoms from the aliphatic tail of organic molecules (Shastri & Huie, 1990; Wayne et

al., 1991; Mora-Diez et al., 2002). In order to investigate this effect as well, kinetic data on the saturated surfactant is then presented in Section 3.4.

3.1. Oleic acid (d_{34}OA) exposed to nitrate radicals (NO_3)

Figure 2 shows the surface excess decays of d_{34}OA monolayers at the air–ACMW interface as a function of time with respect to [NO_3]. The NO_3-initiated oxidation leads to a non-zero surface excess value (7–10 × 10^{13} molecule cm^{-2}) at the end of the reaction. This plateau value is reached after an initial decay, which lasts between 5 min and over 1 h depending on [NO_3]. [NO_3] ranges from (13 ± 6) to (86 ± 45) ppt. For several gas conditions, the oxidation was carried out twice, demonstrating a good reproducibility for high [NO_3] (> 35 ppt), and higher variability for lower concentrations. However, the uncertainty in [NO_3], for [NO_3] < 35 ppt, is ~ 30%, which means that even a small variation in concentration produces a measurable change in the rate of loss of material. For example, such an effect can explain the differences of the d_{34}OA loss rates recorded for [NO_3] = 15 ppt. The oxidant flows in the chamber at t = 0 s, but the decays of the surface excess show a delayed loss most clearly seen at low [NO_3] (black traces with [NO_3] = 13 ppt). The duration of this initial plateau is longer when the oxidant concentration is lower. This suggests that some lenses of oleic acid may be floating on top of the monolayer, and they act as a reservoir for the monolayer until they are totally consumed, then the decay visible by NR relates only to the monolayer. Brewster angle microscopy (BAM) images, recorded while the OA monolayer was compressed, show the appearance of lenses, which are not visible in the expanded phase (see Section 1 of ESI). The surface excess of d_{34}OA was monitored as well for exposure to O_2 and NO_2 in order to assess a mechanical loss due to gas flux and isomerisation effects due to the presence of NO_2 (King et al., 2010).

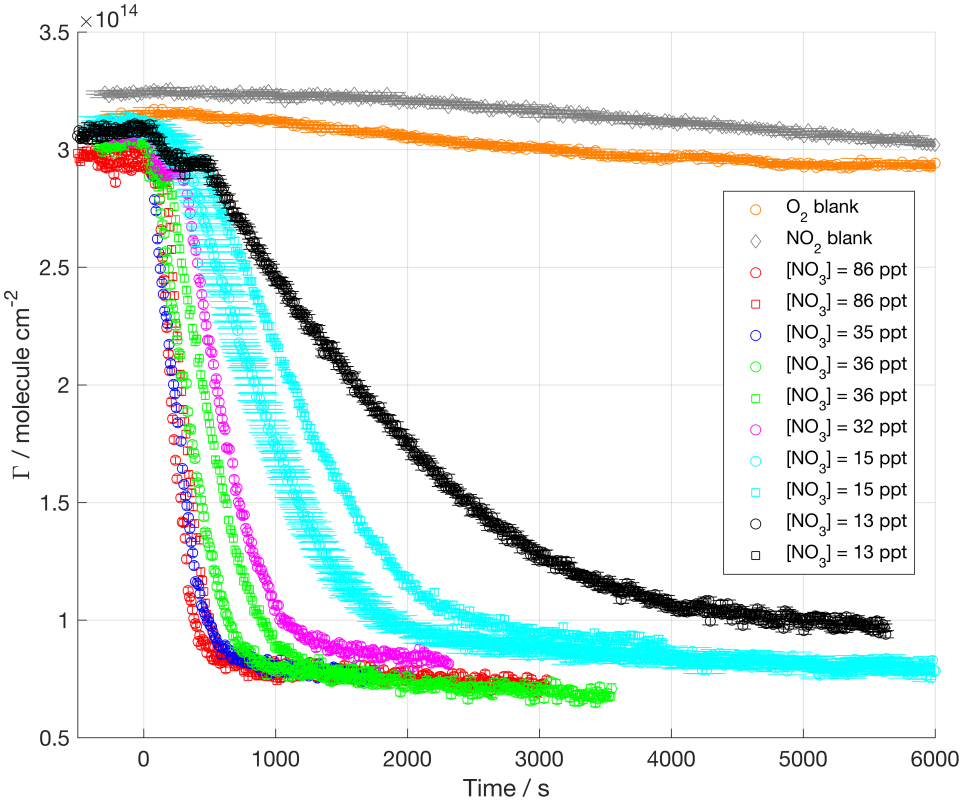

Figure 2. Surface excess decays of oleic acid (d_{34}OA) exposed to different [NO_3]; mean values of NO_3 mixing ratios are displayed in the legend (1 ppt = 2.7 × 10^7 molecule cm^{-3}). NO_3 is admitted at t = 0 s.

The kinetic fitting was performed taking into account the variability of the gas concentrations (both for NO_3 and NO_2) and the initial surface excess was set to a suitable value to take into account the presence of oleic acid droplets and their contribution to products. An example of the kinetic fit is displayed in Figure 3 (see ESI for the complete data set).

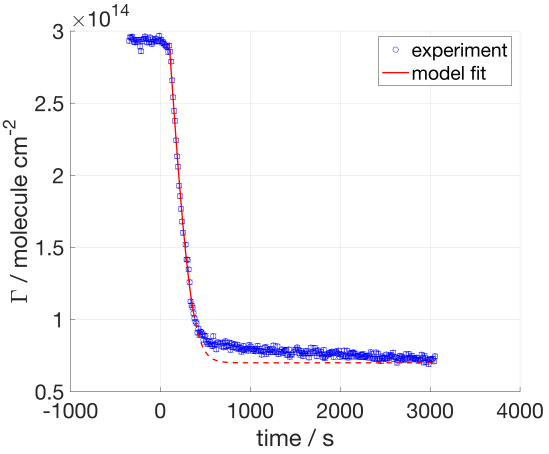

Figure 3. Oleic acid (d_{34}OA) exposed to [NO_3] = 86 ppt. The red line illustrates the fit obtained from our kinetic modelling. The solid section of the red line indicates the data range used for the optimisation of the kinetic parameters; the dashed section of this line illustrates the modelled final part of the decay, but these data were not used in the optimisation of the fitting since below a certain surface excess the molecules rearrange with a different orientation in respect to the interface. The experimental data are displayed with error bars but they are of the same scale as the marker size and hence not very visible; these experimental uncertainties were used in the fitting procedure to calculate the value of χ^2.

The range of data used for the kinetic fitting starts after the initial plateau, and ends at 1×10^{14} molecule cm^{-2}: data below this value are excluded from the fitting for two main reasons: (i) at low coverage the data become more sensitive to experimental details such as the precise background subtraction, so the parameters that affect the kinetic model are better determined without increasing sensitivity to these factors; and (ii) at low coverage some surfactants can segregate into domains which are inhomogeneous laterally, and the NR model does not have the resolution to distinguish this effect but the results are modestly affected, so again it is better to desensitize the kinetic parameters to this effect. The fitted curve, which results from the sum of the surface excesses of d_{34}OA and the products, is shown as a solid red line in Figure 3. Since NR effectively measures the quantity of deuterium atoms at the air–ACMW interface, a distinction between reactant and products is not possible; hence the fitting function needs to take into account the contribution to Γ from both d_{34}OA and its reaction products. In order to determine the product yields, it is assumed that at $t = 0$ s the signal is arising solely from d_{34}OA, while the signal for long reaction time (e.g. $t > 1000$ s for [NO_3] = 86 ppt) is entirely due to the surface-active products. Also, the products (Hung et al., 2005; Docherty & Ziemann, 2006) are assumed to have a similar scattering length density to d_{34}OA, on the basis that upon oxidation the d_{34}OA molecule is expected to break into two parts (Hung et al., 2005; Docherty & Ziemann, 2006), which each maintains almost the same ratio between scattering length and molecular volume. In a first approximation, the scattering length of the products is likely to be half of the scattering length of d_{34}OA and the product film thickness can be thought to be ca. half of the d_{34}OA film thickness. Given that and considering Eq. 2, the resulting surface excess of the products corresponds to the value calculated with ρ, d and b of d_{34}OA. This approximation is not valid in the extreme case of the products being only surface-active, since the packing would be two times denser than that

for oleic acid, and this should be considered in the surface excess calculation and consequent modelling. In our study, the surface-active product yield is 20% and it has been taken into account that the total number of product molecules (surface-active, volatile and soluble) was twice the number of the reactant molecules; we have also estimated the scattering length densities for the likely products.

The accommodation coefficients for the gas-phase species were fixed to one, and the desorption lifetimes were left free to vary in the range 10^{-9}–10^{-7} s, which is in agreement with the values suggested by Shiraiwa et al. (2012b). For the rate coefficient, k_{surf}, the range of variability was optimised through a preliminary sensitivity study performed by changing in the Matlab code the value of k_{surf}. The suitable range of values found was (0.7–4) × 10^{-8} cm^2 molecule^{-1} s^{-1}, which is significantly higher than the best fit value provided by Shiraiwa et al. (2012b) for abietic acid exposed to NO_3 (1.5 × 10^{-9} cm^2 molecule^{-1} s^{-1}). The optimisation of the kinetic parameters was performed systematically by the χ^2 minimisation routine FMINUIT (Allodi). Modelled evolutions of the concentrations of reactants and products are exemplified in Figure 4.

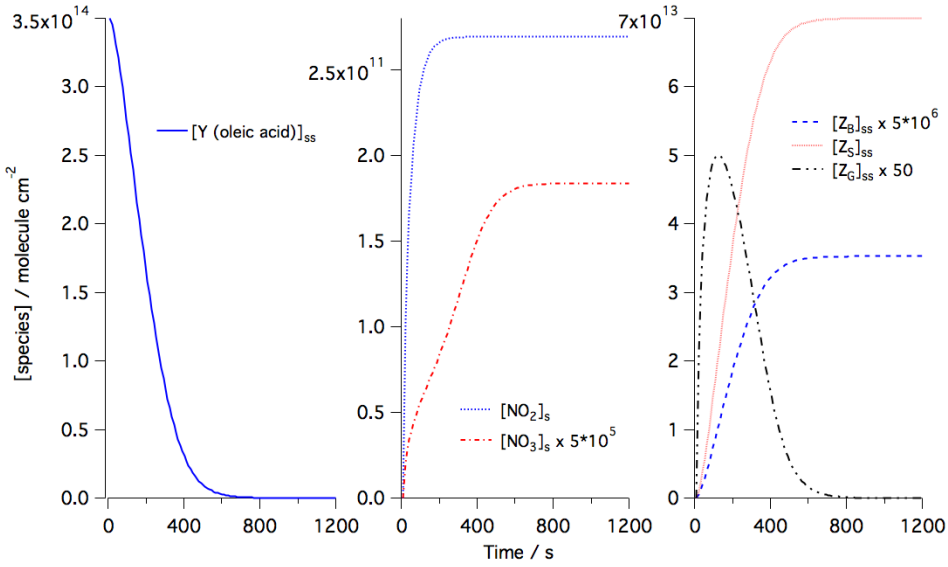

Figure 4. The evolution of the surface concentrations obtained from kinetic modelling using the best-fitted parameters for the data shown in Fig. 3 for (a) the organic reactant (Y) in this case oleic acid; (b) the gas-phase species NO_3 and NO_2; and (c) the surface-active (Z_S), volatile (Z_G) and soluble (Z_B) products.

From BAM images (see ESI) we know that droplets of organic molecules float on top of the monolayer, we need to account for this extra molecules when fitting the model to the experimental data. In fact, the molecules of the monolayer and the droplets are consumed upon oxidation but, until droplets are present, they act as a reservoir and further molecules from the droplets may spread and maintain a constant surface excess until the droplets disappear, leading to the delayed start in decay. The NR signal is averaged over a large surface (cm^2) and it is not sensitive to small droplets (μm) thicker than the monolayer, that is why the surface excess value is constant for this initial part of the decay. To account for this, the initial value for the theoretical $\Gamma(t)$ was adjusted to a higher value than the initial experimental plateau value and the experimental data were considered for fitting after the initial plateau ended (see Figure 5). Figure 5 displays a sensitivity study that demonstrates how the change of desorption lifetimes can affect the model while keeping all the other parameters to the best fit values. A decrease of $\tau_{d,\,NO_3,2}$ slows down the loss rate, especially for the second half of the decay, while an

increase of $\tau_{d,\,NO_3,1}$ speeds up the decay substantially. A decrease in $\tau_{d,NO2}$ does not affect the model significantly ($\tau_{d,NO2}$ was reduced by four orders of magnitude to see any effect in Fig. 5), while an increase slows down the loss rate. Fig. 5 illustrates that the rate coefficients derived through modelling should be quoted together with the desorption lifetimes obtained for the best fit given the substantial impact of changes in the desorption times on the fit to the experimentally observed decays.

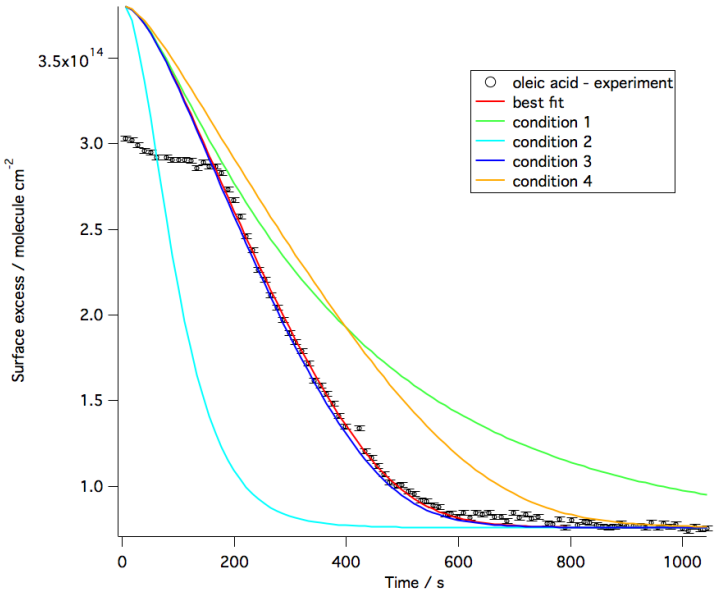

Figure 5. The experimental data for dOA exposed to [NO_3] = 86 ppt are shown with the best fit in red. The desorption lifetimes for NO_3 and NO_2 have selectively been modified in this sensitivity study to show their effect on the modelled surface excess decay. Condition 1 refers to $\left(\tau_{d,\,NO_3,1}\right)_{best\ fit} = \tau_{d,\,NO_3,2}$, and hence $\tau_{d,\,NO_3,2} = \frac{1}{6}\left(\tau_{d,\,NO_3,2}\right)_{best\ fit}$. Condition 2 refers to $\tau_{d,\,NO_3,1} = \left(\tau_{d,\,NO_3,2}\right)_{best\ fit}$ and hence $\tau_{d,\,NO_3,1} = 6\left(\tau_{d,\,NO_3,1}\right)_{best\ fit}$. Condition 3 refers to $\tau_{d,NO2}$=10^{-4} $(\tau_{d,NO2})_{best\ fit}$. Condition 4 refers to $\tau_{d,NO2}$=15 $(\tau_{d,NO2})_{best\ fit}$.

This fitting approach has been applied to all the molecules studied, while accounting for different product yields and kinetic parameter ranges (see Table 2).

A preliminary analysis of the $\Gamma(t)$ profiles was needed to choose the kinetic parameters related to the products, which have been used as fixed input parameters. The product yields were optimised to c_S = 0.2 for the surface-active products, c_G = 0.45 for the volatile products and c_B = 0.35 for the soluble products. The product yields were derived from Docherty & Ziemann (2006); the products were assumed to be hydroxy nitrates, carbonyl nitrates, dinitrates and hydroxydinitrates (Docherty & Ziemann, 2006) as well as a dimer and more highly nitrated compounds from Hung et al. (see products 2a' and 2b' in Hung et al., 2005). A systematic study was performed to determine the effect of the loss of volatile and soluble products on the resulting surface excess profiles. For the volatile products, it was found that a first-order loss rate coefficient, $k_{loss,G}$, above 1×10^{-1} s^{-1} does not change the $\Gamma(t)$ profile and a value of 5×10^{-1} s^{-1} was chosen. For the soluble products, the loss will occur upon diffusion in the sub-phase, hence the relevant parameter is the diffusion coefficient into the bulk water, $D_{b,ZB}$. The calculated $\Gamma(t)$ was affected by the presence of soluble products only for values of $D_{b,ZB}$ below 10^{-14} cm^2 s^{-1}; since no evidence of such an effect was found in the experimental data $D_{b,ZB}$ was fixed to 10^{-7}

$cm^2\ s^{-1}$. The best fit values for the kinetic parameters related to the heterogeneous reaction between d_{34}OA and NO_3 are summarised in Table 2. The rate coefficient for d_{34}OA–NO_3 reaction in presence of NO_2 and O_2 is (2.8 ± 0.7) × 10^{-8} cm^2 $molecule^{-1}$ s^{-1}. The loss due to O_2 and/or NO_2 flows leads to an apparent rate coefficient on the order of 10^{-11} cm^2 $molecule^{-1}$ s^{-1}, which is well within the uncertainty of the reactive rate coefficient. The short desorption time obtained for the best fit for NO_3 is (8.1 ± 4.0) × 10^{-9} s and the slow desorption is about three times longer, similar to the NO_2 desorption time. The introduction of two desorption times reflects the change of orientation of the organic molecules at the interface, i.e. for a highly packed monolayer the reactive site is assumed to be less accessible, and the oxidant has less affinity for other parts of the molecules hence the desorption is faster. When the organic surface coverage decreases the reactive sites become more accessible and the desorption is slowed down. The effect of the two desorption time on the $[NO_3]_s$ evolution is visible in Figure 4, where the increase of $[NO_3]_s$ shows a different slope from 200 s once the oleic acid surface excess halved (compare to Eq. 7). Figure 4 shows the time evolution of the surface concentrations of reactants, products and gas-phase species; once the reactant, d_{34}OA, is completely consumed all the other species reach a steady state.

Table 2. Results of the kinetic modelling of the experimental data for the d_{34}OA–NO_3, d_{14}POA–NO_3, d_{33}MO–NO_3 and d_{35}SA–NO_3 systems. The uncertainties correspond to one standard deviation.

	Best fit values			
Modelled parameter	**d_{34}OA**	**d_{14}POA**	**d_{33}MO**	**d_{35}SA**
k_{surf} / 10^8 cm^2 $molecule^{-1}$ s^{-1}	2.8 ± 0.7	2.4 ± 0.5	3.3 ± 0.6	(5 ± 1) × 10^{-4}
(constraints)	(0.7 – 4)	(1 – 3)	(0.7 – 4)	(10^{-4} – 4)
$\tau_{d,NO3,1}$ / 10^9 s	8.1 ± 4.0	16 ± 4.0	8.1 ± 3.0	18.2 ± 0.4
(constraints)	(5 – 20)	(5 – 20)	(5 – 20)	(5 – 20)
$\tau_{d,NO3,2}$ / 10^8 s	2.3 ± 0.8	3.1 ± 1.3	3.7 ± 1.3	[0.70 ± 0.01][a]
(constraints)	(0.7 – 4)	(1 – 6)	(1 – 5)	(0.7 – 4)
$\tau_{d,NO2}$ / 10^8	2.8 ± 1.6	4.7 ± 2.0	2.9 ± 2.0	4.7 ± 0.4
(constraints)	(0.1 – 6)	(0.1 – 6)	(0.1 – 6)	(0.1 – 6)

[a] $\tau_{d,NO3,2}$ corresponds to the lower limit of the constrained range; in this system the surface excess does not halve in the experimentally accessible timeframe and hence $\tau_{d,NO3,2}$ is not accurately determined.

3.2. Palmitoleic acid (d_{14}POA) exposed to nitrate radicals (NO_3)

NO_3-initiated oxidation of POA monolayers at the air–water interface was studied as described above for OA. 14 deuterium atoms were present between the carbon double bond and the carboxylic group in the partially-deuterated d_{14}POA sample used. POA has a chemical structure that is similar to OA. In fact the portion from the carboxylic acid to the C=C bond is exactly the same, while the remaining part of POA chain has just five CH_2 units compared to the seven CH_2 units present in the corresponding part of the OA chain. The key reactive site (C=C) for NO_3-initiated oxidation is in a similar chemical environment, but the products formed and their fates may be different. Products are expected to be analogous to those formed by oleic acid, except that they should be slightly more volatile since the alkyl chain is shorter.

Figure 6 shows the surface excess decays of d_{14}POA monolayers at the air–ACMW interface as a function of time with respect to $[NO_3]$. The reaction leads to a non-zero surface excess in the range 3 – 7 × 10^{13} molecule cm^{-2}, which is slightly lower than the value found for d_{34}OA; this suggests that a proportion of the surface-active products is formed of hydrogenous material and hence has a low scattering contrast to the neutron probe. The proportion of molecules remaining stably at the interface in relation to the number of initial reactant molecules is

15% for d_{14}POA while it is 20 to 25% for d_{34}OA (depending on which initial surface excess value is used, fitted or measured). On the assumption that the double bond is the reactive site and breaks during the oxidation process, the partial deuteration of the d_{14}POA (as opposed to the full deuteration of d_{34}OA) may in fact help in determining which part of the molecule remains at the interface: 5–10% of the surface-active products appear to originate from the alkyl chain not connected to the acidic head group in the d_{34}OA system (however, a direct proof would require for half-deuterated d_{34}OA and/or fully deuterated d_{14}POA to become available for additional oxidation experiments).

For low oxidant concentrations ([NO_3] < 32 ppt), the final plateau value was not always reached (although it was reached for the slowest reaction) because the reaction had to be stopped prematurely due to time constraints of beam time experiments. Compared to d_{34}OA, the decay signals are more noisy, which is due to the half deuteration leading to a weaker contrast and hence lower signal to noise ratios. The decays of surface excess start as soon as NO_3 is admitted to the chamber and no initial plateau is visible (as was the case for some of the d_{34}OA decays displayed in Figure 2). No lenses were formed in this system, as was confirmed by recording BAM images while the POA monolayer was compressed (see ESI).

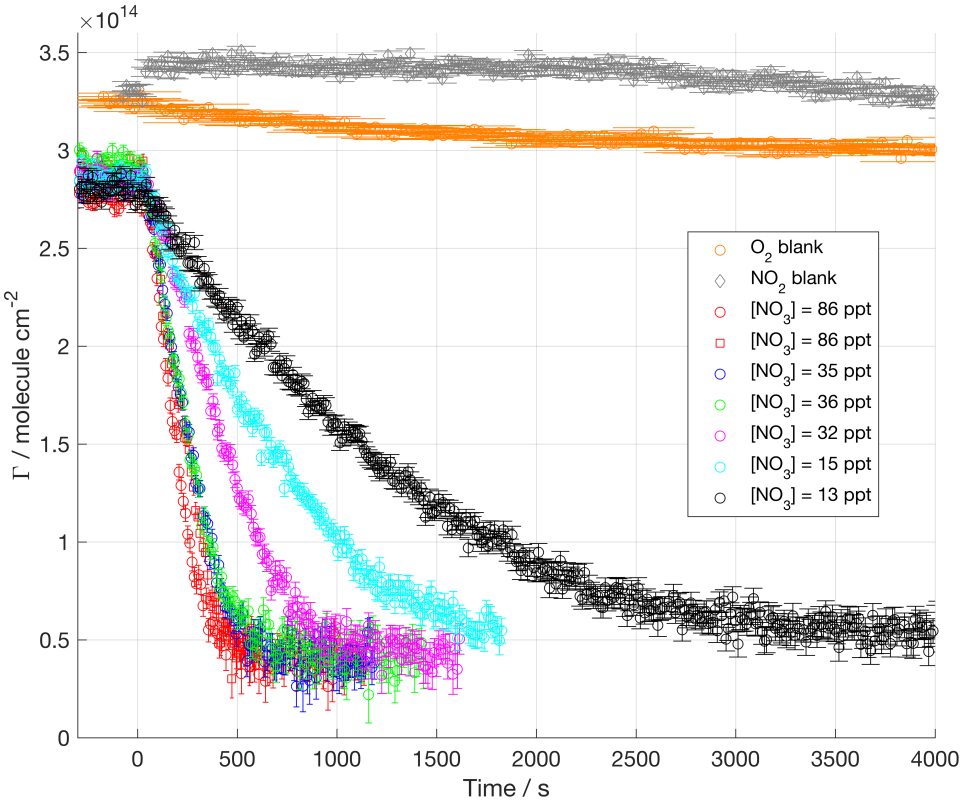

Figure 6. Surface excess decays of palmitoleic acid (d_{14}POA) exposed to different [NO_3]; mean values are displayed in the legend. NO_3 exposure is started at t = 0 s. The experimental data are more scattered than those for d_{34}OA, because the d_{14}POA was half-deuterated (*i.e.* 14 D atoms, see Table 1 in ESI) leading to a weaker contrast (*i.e.* lower signal-to-noise ratio) compared to the fully deuterated molecules studied.

The kinetic analysis was performed as described for d_{34}OA. The input parameters for description of the products were c_S = 0.17, c_G = 0.48 and c_B = 0.35, the surface-active and volatile product yields were adjusted to match the residual surface excess; please note that hydrogenous surface-active products are not taken into account in this

context since the experimentally observed signal originates exclusively from the deuterated part of the POA molecules. The variable parameters were constrained to the following value ranges: k_{surf} was allowed to vary (1 – 3) × 10^{-8} cm^2 $molecule^{-1}$ s^{-1}, $\tau_{d,NO3,1}$ varied between (5 – 20) × 10^{-9} s, $\tau_{d,NO3,2}$ varied between (10 – 60) × 10^{-9} s and $\tau_{d,NO2}$ varied between (0.1 – 6) × 10^{-8} s (see Table 2).

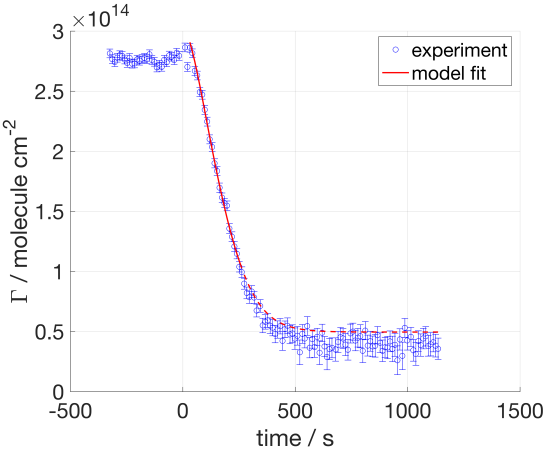

Figure 7. Palmitoleic acid (d_{14}POA) exposed to [NO_3] = 86 ppt. The red line illustrates the fit obtained from our kinetic modelling (the solid section of the line indicates the data range used for the kinetic analysis; the dashed section of the model line illustrates the calculated final part of the decay, but the corresponding experimental data were not used in the optimisation of the fitting).

In Figure 7 an example of the model fitted to d_{14}POA data is displayed; the decay is very well represented by the model. The results of the kinetic modelling for d_{14}POA are presented in Table 2. While the rate coefficient is similar to the value found for d_{34}OA (Table 2), $\tau_{d,NO3,1}$ is double of the value found for oleic acid, this lifetime refers to the monolayer when is highly packed (see description in Section 2.2) and that is the condition where the difference in chain length between d_{14}POA and d_{34}OA can play a role. The higher value of $\tau_{d,NO3,1}$ for d_{14}POA is consistent with the hypothesis of an easier access to the double bond due to the shorter alkyl chain of d_{14}POA. The $\tau_{d,NO3,2}$ does not show a big difference between d_{14}POA and d_{34}OA and that refers to the monolayer in a less dense state, suggesting that once the access to the double bond is comparable the reaction has a similar behaviour for the two molecules. d_{14}POA surface excess data have larger experimental errors than the fully deuterated molecules.

3.3. Methyl oleate (d_{33}MO) exposed to nitrate radicals (NO_3)

Methyl oleate possesses the same aliphatic chain as OA, but it has a different head group: instead of a carboxylic acid it has a methyl ester ($COOCH_3$) group. Fully deuterated d_{33}MO was used (see Table 1 in the ESI). MO occupies a larger surface area and is less stable at the air–water interface than OA because of its less hydrophilic head group (see isotherm in Section 1 of the ESI). However, the reactive site is in a similar chemical environment as for OA, and any difference in reaction kinetics is expected to be related to the chain orientation and formation of different products.

Figure 8 displays the surface excess decays of d_{33}MO monolayers at the air–ACMW interface as a function of time with respect to [NO_3]. [NO_3] was varied from (13 ± 6) ppt to (86 ± 45) ppt.

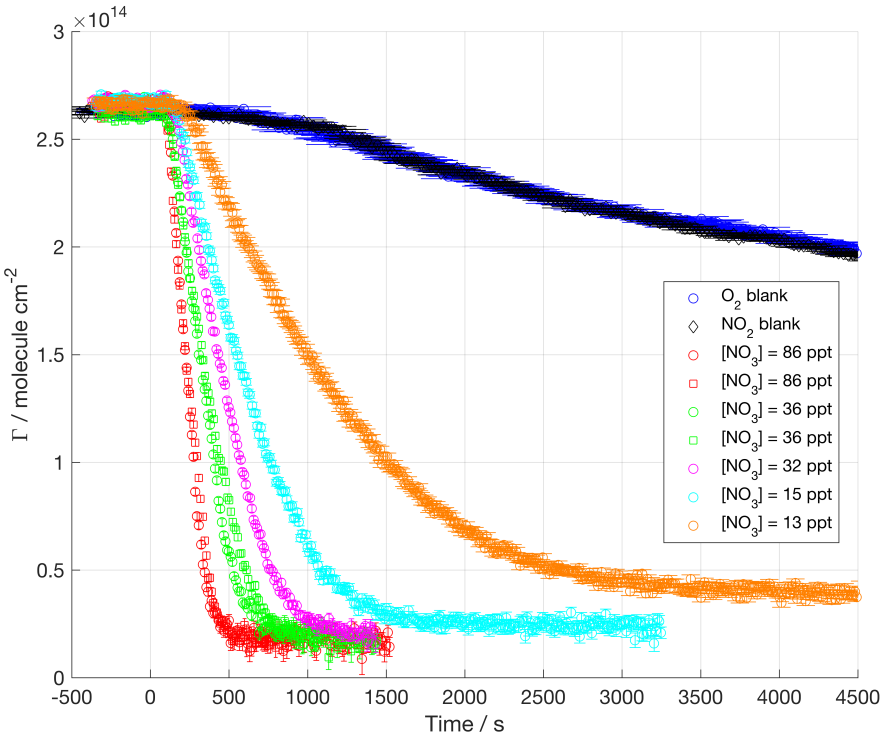

Figure 8. Surface excess of methyl oleate (d_{33}MO) exposed to different [NO_3], mean values are displayed in the legend. NO_3 exposure is started at $t = 0$ s.

The kinetic decays presented in Figure 8 show a very clear dependence on [NO_3] and very good signal-to-noise ratios. The decays are generally faster than for both d_{34}OA and d_{14}POA. The exposure to O_2 and NO_2 flow leads to similar surface excess decays; this non-reactive loss is significantly larger than those recorded for d_{34}OA and d_{14}POA suggesting that d_{33}MO is not as stable at the air–water interface as d_{34}OA and d_{14}POA. The apparent rate coefficient obtained for the decays in absence of NO_3 is about 2×10^{-10} molecule cm^{-2} s^{-1}. As for d_{34}OA, the reaction starts with a slightly increasing delay as the oxidant concentration is lower; the formation of droplets floating on top of the monolayer after spreading could explain this effect, since the compound is liquid at room temperature and evidence of lenses was found in BAM images (see Section 1 in the ESI). The minimum value reached by the surface excess is $\approx 2 \times 10^{13}$ molecule cm^{-2}, which is at the detection limit. Therefore, no surface-active products are expected to remain at the interface as was also found in ozonolysis experiments with d_{33}MO in the same chamber (Sebastiani et al., 2015); this was also confirmed by complementary ellipsometry measurements in the same reaction chamber (data not shown). According to this finding, the product yields were chosen as follows: $c_S = 0.03$, $c_G = 0.45$ and $c_B = 0.52$. The c_s value was set to 0.03 in order to account for the surface excess detection limit considering the experimental background. The kinetic parameters were constrained to the following value ranges: k_{surf} was allowed to vary $(0.7 – 4) \times 10^{-8}$ cm^2 molecule^{-1} s^{-1}, $\tau_{d,NO3,1}$ varied between $(5 – 20) \times 10^{-9}$ s, $\tau_{d,NO3,2}$ varied between $(10 – 50) \times 10^{-9}$ s and $\tau_{d,NO2}$ varied between $(0.1 – 6) \times 10^{-8}$ s (see Table 2). An example of the fitting resulting from the kinetic modelling is displayed in Figure 9. The best-fit values obtained from the kinetic model are presented in Table 2. The rate coefficient for d_{33}MO is slightly larger than those for both d_{34}OA and d_{14}POA, while the desorption times are similar to those found for d_{34}OA and d_{14}POA with the exception of the doubled $\tau_{d,NO3,1}$ for POA further confirming the better accessibility of the double bond for the shorter chained POA compared to both OA and MO. All fits are presented in the ESI.

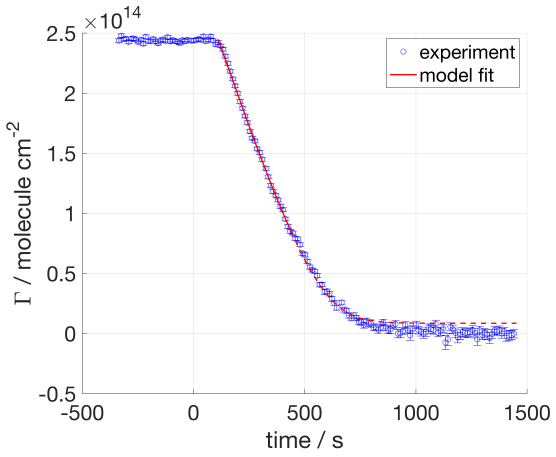

Figure 9. Methyl oleate (d_{33}MO) exposed to [NO_3] = 36 ppt. The red line illustrates the fit obtained from our kinetic modelling (the solid section of the line indicates the data range used for the kinetic analysis; the dashed section of the model line illustrates the calculated final part of the decay, but the corresponding experimental data were not used in the optimisation of the fitting).

3.4 Stearic acid (d_{35}SA) exposed to nitrate radicals (NO_3)

In addition to adding to the double bond of the unsaturated surfactants discussed in the previous sections, NO_3 may abstract hydrogen atoms from the aliphatic tail (Shastri & Huie, 1990; Wayne et al., 1991; Mora-Diez et al., 2002). In order to investigate the contribution of this hydrogen abstraction, the saturated surfactant stearic acid was exposed to NO_3. Figure 10 shows the comparison between the surface excess of a d_{35}SA monolayer exposed to O_2 and to NO_3 at (86 ± 45) ppt.

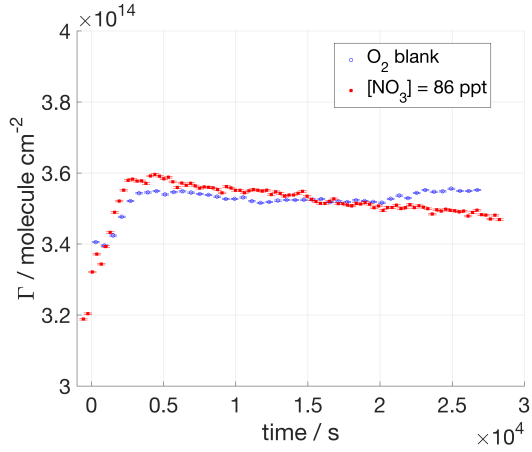

Figure 10. Surface excess of stearic acid (d_{35}SA) exposed to O_2 (blue circles) and to [NO_3] = 86 ppt (red filled squares). Exposure to NO_3 starts at t = 0 s. Both surface excess traces show an increase over the first 40 min. There is slight subsequent decrease in the surface excess during exposure to NO_3.

The data were recorded for more than 8 h for both gas-phase environments. The initial surface excess evolution of the monolayer exposed to NO_3 is comparable to that for the O_2 blank: both profiles show a slow increase in surface excess in the first 40 min. Apart from the initial increase in $\Gamma(t)$ values, no measurable change in the surface excess has been recorded when SA is exposed to O_2, and the film is shown to be stable on the probed time scale; in presence of NO_3 a slight decrease in surface excess hints at a slow reactive decay. From these data we estimated a rate coefficient, k_{surf}, of approximately (5 ± 1) × 10^{-12} cm^2 $molecule^{-1}$ s^{-1}; the parameters ranges and initial values in the model were kept as for OA for consistency, because of the lack of any experimental data

on products and very limited kinetic data due to the very slow process; the lower limit for the rate coefficient was decreased to 1×10^{-12} cm^2 molecule^{-1} s^{-1}; the model fit to the experimental data is displayed in the ESI; the estimated kinetic parameters should be considered with caution given the severe limitations mainly due to the lack of experimental data. For this system, the surface coverage never reached below 90% of the initial value and hence the determination of the second desorption times, $\tau_{d,NO3,2}$, is not accurate (the value obtained for $\tau_{d,NO3,2}$ actually corresponds to the lower limit of the constrained range; see value in square brackets in Table 2). It should be noted that in our experimental approach it is theoretically possible that the chemical composition of the monolayer could change upon reaction with NO_3 (e.g. formation of organonitrates; Gross & Bertram, 2009) while the scattering excess (i.e. the product of ρ and d in Eq. (2)) could by coincidence remain unchanged during this process; the resulting $\Gamma(t)$ plot would then also remain constant. This is highly unlikely, in particular since our result is in accordance with the findings of Knopf et al. (2006), where the exposure to $[NO_3] = 100$ ppt for one week resulted in a maximum of 10% of the organic monolayer being volatilised (the monolayer was supported on a solid substrate and the measurement does not rely on the neutron scattering length density). For practical reasons it is not feasible to carry out NR experiments on a similar time scale, however our results suggest that the kinetic behaviour may be affected by the type of substrate given the faster oxidation of d_{35}SA observed at the air–water interface during exposure to NO_3.

4. Discussion

The kinetic parameters obtained by analysing the NR data allow investigation of the effects of the chemical structure, i.e. chain length, degree of unsaturation and head group properties. A summary of the kinetic results reported in the present study is given in Table 3. For the unsaturated molecules studied we obtained rate coefficients in the order of 10^{-8} cm^2 molecule^{-1} s^{-1}, which leads to uptake coefficients, γ, for NO_3 on a droplet covered in a monolayer of organic compound to be in the order of 10^{-3}. These results broadly agree with the very limited number of measurements found in the literature (Moise et al., 2002; Knopf et al., 2006; Gross & Bertram, 2009; Xiao & Bertram, 2011; Zhao et al, 2011; Zhang et al., 2014b) for unsaturated organics exposed to NO_3 in particular when considering that experiments are often carried out in very different conditions (e.g. on a gold surface instead of the water surface we used) and employ fundamentally different experimental approaches (e.g. flow tubes). Moise et al. (2002) studied the uptake of NO_3 by a range of liquid or frozen organics in a rotating wall flow tube, and they measured uptake between 1.6×10^{-3} and 1.5×10^{-2} depending on the kind of liquid organic compounds. Gross & Bertram (2009) determined the uptake of NO_3 by a self-assembled alkene monolayer at the solid substrate obtaining an uptake coefficient of 0.034. They suggested that a possible reason for this higher value compared to the results of Moise et al. (2002) is the location of the double bond at the interface. Zhang et al. (2014b) determined the uptake coefficient of NO_3 on a model surface of a self-assembled monolayer of vinyl-terminated alkanethiols on gold substrate to be $(2.3 \pm 0.5) \times 10^{-3}$ monitoring the double bond rupture. The present results for organic monolayers at the air–water interface are in a better agreement with those of Moise et al. (2002) and Zhang et al. (2014b). The agreement with Moise et al. (2002) may suggest that the accessibility of the reactive site for these monolayers is similar to that of a thick film. However, the work of Zhang et al. (2014b) was on an organic monolayer at the air–solid interface and the rate of product formation was measured instead of the NO_3 consumption as in Gross & Bertram (2009); in a way our approach is closer to that of Zhang et al. (2014b), since we followed the organic reactant loss *in situ*. Given the

complex chemical environments these surfactants will encounter in the atmosphere it would be important to investigate the difference in uptake coefficients of NO_3 by organic monolayers adsorbed to different substrates and compare uptake coefficients based on both consumption of NO_3 and product formation rates. King et al. (2009) investigated OA oxidation by O_3 on different subphases with pH ranging from 2 to 7 and no significant change was found in the rate coefficient. In our experiments with the oxidant NO_3 we expect HNO_3 to be formed, and induce a change in pH in the subphase, but given the fact that it was previously reported that there was no pH effect, we did not explore the pH changes in the present study.

Table 3. Kinetic parameters, uptake coefficients and estimated monolayer lifetimes for the compounds studied. Literature values for uptake coefficients on similar compounds are included for comparison.

Surfactant	k_{surf} / cm^2 molecule^{-1} s^{-1}	γ / 10^3	γ_{lit} / 10^3	Lifetime[a]
d_{35}SA	$(5 \pm 1) \times 10^{-12}$	$(5 \pm 1) \times 10^{-4}$	$(8.8 \pm 2.5) \times 10^{-1}$ [b]	21 days
d_{34}OA	$(2.8 \pm 0.7) \times 10^{-8}$	2.1 ± 0.5	$(3 \pm 1) \times 10^{2}$ [c] $[1.6 \pm 0.3]$ [d]	6 minutes
d_{14}POA	$(2.4 \pm 0.5) \times 10^{-8}$	1.7 ± 0.3	$[2.3 \pm 0.5]$ [e] $[34^{+44}_{-18}]$ [f]	7 minutes
d_{33}MO	$(3.3 \pm 0.6) \times 10^{-8}$	2.1 ± 0.4	$[(1.4^{+8.6}_{-0.5}) \times 10^{2}]$ [g]	5 minutes

[a] see Section 4.3 for details on the lifetime calculation;
[b] value refers to a self-assembled monolayer on a gold substrate (Knopf et al., 2006);
[c] value refers to a study with a flow tube coupled to a chemical ionisation mass spectrometer (Zhao et al., 2011);
[d] value refers to 1-octadecene uptake measured in a rotating wall flow tube (Moise et al., 2002);
[e] value refers to a vinyl-terminated self-assembled monolayer at a gold surface, which was chosen as a model for a double bond positioned at the gas–surface interface by Zhang et al. (2014b);
[f] value refers to a terminal alkene monolayer at a gold surface (Gross & Bertram, 2009);
[g] value refers to binary mixtures of MO and saturated molecules measured in a rotating wall flow tube (Xiao & Bertram, 2011).

The products yields used in our model were based on the findings of Docherty & Ziemann (2006) and Hung et al. (2005); both papers present possible mechanisms for product formation from the oleic acid droplets reacting with NO_3 in presence of O_2 and NO_2. NO_3 attacks the double bond and the primary reaction is most likely to lead to the formation of an organonitrate, which would maintain the C_{18} chain instead of splitting into C_9 fragments; however, subsequent reactions have been found to lead to shorter molecules, such as nonanal and 9-oxononanoic acid (Docherty & Ziemann, 2006). Organonitrates are reactive species that are likely to undergo further reactions and produce smaller fragments, which either are lost to the gas- or water-phase or remain at the interface. In previous work (Hung et al., 2005; Docherty & Ziemann, 2006), the primary organonitrates were found to be more abundant than shorter fragments, but these studies focused mostly on the first few seconds to minutes of the reactive degradation, while our work on unsaturated surfactants follows the reaction until the organic film is fully processed. The surface-active products were found to total 20% and 15% (based on the deuterated proportion of the molecule only) of the initial amounts of d_{34}OA and d_{14}POA, while d_{33}MO does not lead to any surface-active products ($\leq$ 3%), probably due to the lower surface activity of the $COOCH_3$ head group. The proportion of volatile and soluble products is mainly based on solubility and volatility estimations (Kuhne et al., 1995; Compernolle et al., 2011); this distinction was used to predict the time evolution of the concentrations of these products and their contribution to the surface excess when produced at the interface. d_{14}POA is expected to behave similarly to d_{34}OA, except the formation of C_8 fragments with slightly higher solubility & volatility and hence a decreased surface-active yield; to our knowledge no studies on d_{14}POA exposed to NO_3 were performed

and no data are available on the products formed. For all the reactions studied here we expect secondary reactions not to be significant due to our set-up with a one-molecule thin layer of organic molecules each containing only a single reactive site (NO_3-initiated hydrogen abstraction is much slower than addition to the double bond as demonstrated in our work on the oxidation of the saturated surfactant stearic acid). Multiple generations of oxidation products could not be resolved in this experimental approach and are not considered explicitly in this work. Simultaneous neutron reflectometry and infrared reflection absorption spectroscopy (IRRAS), a technique we have recently developed for study of related systems (Skoda et al., 2017) may be able to give some information on the chemical composition of one-molecule thin films during kinetic studies of oxidation reactions at the air–water interface in the future.

Although our present approach did not allow convenient variation of the surface excess due to the barrier-less Langmuir trough in our miniature kinetic chamber optimised for kinetic measurements of fast reactions (Sebastiani et al., 2015), we believe that the best fit parameters we report in the present study can predict the fate of an organic monolayer with a different compression, i.e. at a different initial surface excess.

The key findings of the present work in relation to surfactant chain length, head group and saturation are discussed in the following paragraphs.

4.1. Chain length

The slightly lower rate coefficient of d_{14}POA compared to d_{34}OA is hard to rationalise (the rate coefficients obtained overlap with the experimental uncertainties), since –if anything– we would have expected d_{14}POA to react slightly faster given the fact that the two molecules are identical except a shorter alkyl chain that could facilitate attack of NO_3 in the case of d_{14}POA (as seems to be the case for O_3 attack on OA and POA in a complex 12-component mixture containing these two compounds: Huff Hartz et al. (2007) reported ratios of effective condensed phase rate constants of 7 ± 3 and 6 ± 2 for POA and OA ozonolysis, respectively; no kinetic measurements have been reported for the d_{14}POA–O_3 system to our knowledge). However, the reactivity depends on the desorption time as well (Table 2); the longer the lifetime of adsorption, the higher is the possibility to react; $\tau_{d,NO3,1}$ for d_{14}POA is double the value found for d_{34}OA, which confirms the hypothesis of an easier access to the double bond due to the shorter alkyl chain of d_{14}POA.

The uncertainty of the rate coefficient corresponds to the standard deviation of the values found for the rate coefficients for each oxidant concentration; a lower uncertainty means that the values obtained from the different oxidant concentrations are closer to each other. Since the rate coefficients obtained for the individual experiments for d_{14}POA agree slightly better than those for the other surfactant reactions, a smaller χ^2 is obtained despite the clearly visible scatter in the d_{14}POA surface excess profiles (see Fig. 6) and the larger error bars on the data.

4.2. Head group

The rate coefficients displayed in the second column of Table 3 for the reactions with NO_3 show a small, but statistically significant difference between the unsaturated organic compounds investigated: d_{33}MO reacts

slightly faster than d_{34}OA with d_{14}POA reacting the slowest. This order of reactivity is broadly consistent with that found for the ozonolysis of *d*MO (Pfrang et al., 2014; Sebastiani, et al., 2015) and d_{34}OA (King et al., 2009) at the air–water interface, but the differences are less pronounced for the more reactive NO_3: $k_{surf,NO3}$ / $k_{surf,O3}$ ratios are ~ 384 and ~ 58 for d_{34}OA and d_{33}MO, respectively.

A direct comparison between surface excess decays for the three unsaturated surfactants allows us also to examine if there is a correlation between the type of head group and the presence of products at the air–water interface. Molecules with a fatty acid (COOH) head group (i.e. d_{34}OA and d_{14}POA) left a considerable proportion of surface-active products at the air–water interface, while d_{33}MO with its methyl ester ($COOCH_3$) head group did not leave any detectable product ($\leq$ 3% surface-active products based on the detection limit for our experimental set-up). Therefore, the retention of the organic character at the air–water interface differs fundamentally between the different surfactant species: the fatty acids studied form products with a yield of ~ 20% that are stable at the air–water interface while the NO_3-initiated oxidation of the methyl ester rapidly removes the organic character from the surface of the aqueous droplet. A similar difference (King et al., 2009; Pfrang et al., 2014; Sebastiani et al., 2015) between methyl ester and parent fatty acid has been found for the ozonolysis of d_{34}OA and d_{33}MO, but the retention of 20% of organic material at the air–water interface is even more surprising for the more highly reactive nitrate radicals. The film-forming potential of the reaction products thus strongly depends on the head group properties.

4.3. Chain saturation

Unsurprisingly, the fate of the monolayer is altered fundamentally by the absence of unsaturation in the aliphatic chain. In fact, d_{35}SA loss from the interface during our 8 h experiments was extremely small, while the initial 40 minutes of reaction lead to an increase of surface excess for both NO_3 and O_2. An increase in surface excess may depend on a closer packing of the aliphatic chains that is more likely than gas-phase species absorbing to the interface, since gas absorption was not found for the other molecules studied. Indeed, we have recently reported an apparent increase in NR signal most likely caused by changes in the structure at the air–water interface for a two-component mixture of immiscible surfactants (Skoda et al., 2017). Our implementation of NR only at low-q provides a measure of the total neutron scattering excess rather than a direct measure of the surface excess of the organic material at the interface hence there is a possibility that the film composition may be changing over time due to gas adsorption into the monolayer, e.g. formation of organonitrates by NO_3 (Gross & Bertram, 2009). Due to limited access to neutron beam time, only one experiment was performed on d_{35}SA lasting 8 h and it led to an estimation of the rate coefficient of $(5 \pm 1) \times 10^{-12}$ cm^2 molecule^{-1} s^{-1}, which is four orders of magnitude lower than the rate coefficient for the unsaturated molecules. This value has to be considered with caution, since it relies on the modelling of only one data set, corresponding to the highest NO_3 concentration, and the parameters in the modelling were the same as for d_{34}OA except for the lower limit of the rate coefficient that has been reduced to 1×10^{-12} cm^2 molecule^{-1} s^{-1}. This was necessary because of the lack of previous experimental data to constrain the model and the limited reaction extent that could be observed during the available beam time.

The higher stability of SA monolayers upon oxidation compared to the unsaturated molecules suggests that SA may concentrate at the aerosol surface leading to a stabilisation of the particles. Formation of such a stable film

may protect more reactive species, located within the aerosol bulk (Pfrang et al., 2011), by slowing down the diffusion of the organic compound from bulk to surface and the diffusion of the oxidant from the gas phase to the bulk. Accumulation of saturated films in aged organic films has indeed recently been reported (Jones et al., 2017).

4.4. Atmospheric implications

Contrasting the oxidation of d_{33}MO upon exposure to O_3 (Pfrang et al., 2014; Sebastiani, et al., 2015) and NO_3 shows –as expected– a clearly stronger oxidative power of NO_3 compared to O_3. The oxidative power may be quantified from the uptake coefficient (Gross & Bertram, 2009) of NO_3 and O_3 as the product of uptake coefficient and gas-phase oxidant concentration. O_3 is found in the atmosphere at concentration between 10 and 100 ppb. The oxidative power calculated for the lowest concentration would be 7.5×10^6 molecule cm^{-3}. For the calculation of the oxidative power, $[NO_3]$ was chosen to be representative of a range of atmospheric mixing ratios (5–50 ppt, i.e. ca. $1.4–13.5 \times 10^8$ molecule cm^{-3}), which could be encountered in the atmosphere owing to spatial and seasonal fluctuations (Seinfeld & Pandis, 2006). The resulting oxidative powers are 1.2×10^6 molecule cm^{-3} and 12×10^6 molecule cm^{-3} for lowest and highest $[NO_3]$, respectively. Although the concentration of NO_3 in the atmosphere is low compared to $[O_3]$, our results suggest that night-time oxidation is likely to be often dominated by NO_3-initiated degradation. This finding suggests that further investigation of the oxidation driven by NO_3 is required to understand the fate of aerosol droplets together with studies of the key daytime oxidant OH. This conclusion is also supported by a very recent study (Jones et al., 2017) suggesting that atmospheric surfactants are essential inert with respect to ozonolysis making studies of NO_3 as well as OH-initiated oxidation even more timely.

The lifetime of an organic monolayer is calculated (Moise & Rudich, 2001; Knopf et al., 2011) as the inverse of the product of k_{surf} and $[NO_3]_s$, the NO_3 surface concentration was calculated as in Smith et al. (2002) using a $[NO_3] = 20$ ppt (5.4×10^8 molecule cm^{-3}). Based on our kinetic experiments, the lifetime with respect to NO_3-initiated oxidation of an organic monolayer of monounsaturated molecules with a surface concentration of 3×10^{14} molecule cm^{-2} on an aqueous droplet is ca. 5 to 7 minutes, while it becomes about 21 days for saturated species. Zhao et al. (2011) estimated for a 100 nm droplet of pure oleic acid exposed to 25 ppt NO_3 a lifetime of ca. 35 minutes. The direct comparison with our kinetic study on a self-assembled monolayer at the air–water interface suggests that oleic acid molecules in a pure oleic acid droplet would be degraded ca. 20 times faster than the same number of oleic acid molecules present in a self-assembled monolayer at the air–water interface of an aqueous droplet. Self-assembly thus may play a significant role for the kinetic behaviour of surfactant molecules in the atmosphere. We are currently carrying out experimental studies on oleic-acid based aerosol proxies with complementary techniques (Seddon et al., 2016) to further investigate the importance of complex self-assembly in atmospheric aerosols (Pfrang et al., 2017).

The loss of the organic character from the air–water interface will have consequences for the surface tension of aqueous droplets in the atmosphere: an organic surfactant film substantially reduces the droplet's surface tension compared to pure water, so that the film-forming potential of degradation products of these surfactant films is of key interest. We found that the stability of products formed at the air–water interface differs substantially

between the fatty acids (OA and POA) and the methyl ester (MO) studied. The head group thus seems key to determine whether the surfactant will be able to reduce the surface tension of water droplets for any considerable time which could have important consequences for droplet growth and should be considered when developing emission control strategies.

The rapid loss of the organic monolayers at the air–water interface demonstrated by our experimental data of the oxidative decays is surprising given a number of field studies reporting much longer residence times of unsaturated surfactants in atmospheric aerosols (Morris et al., 2002; Knopf et al., 2005; Ziemann, 2005; Zahardis & Petrucci, 2007). Such unsaturated organics may have longer lifetimes if protected from oxidative attack by gas-phase species e.g. inside highly viscous aerosol particles (Virtanen et al., 2010; Pfrang et al., 2011; Shiraiwa et al., 2011; Shiraiwa et al., 2013) or if mixed with non-reactive species in a complex surface film with yet unexplored kinetic behaviour. This provides a key motivation to investigate the oxidation of mixed surfactant films, which represent closer proxies for real atmospheric aerosol droplets in the future. These measurements have commenced already in our group, and as such the findings presented here provide an essential experimental basis for an extension of the work and methodology towards an improved understanding of the complex behaviour of atmospheric aerosols.

5. Conclusions

We have investigated the reactions of the key atmospheric oxidant NO_3 with organic monolayers at the air–water interface as proxies for the night-time ageing of organic-coated aqueous aerosols. The surfactant molecules chosen allowed the investigation of the effects of chain length, head group properties and degree of unsaturation on the reaction kinetics as well as the proportion of surface-active products formed. The experimental results presented together with the tailored modelling approach for the four structurally different monolayers has allowed determination of the kinetic parameters of heterogeneous reactions at the air–water interface with NO_3 for the first time. The study of heterogeneous reactions of organic monolayers at the air–water interface exposed to oxidants is crucial to understand the role of such films for the atmospheric fate of organic-coated aqueous aerosols (Gilman et al., 2004). Previous studies performed on these types of reactions were nearly exclusively carried out monitoring the gas-phase species (Wadia et al., 2000; Knopf et al., 2007; Cosman et al., 2008a; Cosman et al., 2008b). Gross & Bertram (2009) investigated the oxidation of organic monolayers at an air–solid interface and in addition to monitoring the gas-phase species during the reaction, they analysed the product film with several surface spectroscopic techniques. The monitoring of the organic monolayer during oxidation at the air–water interface was introduced by King et al. (2009) for the study of OA exposed to O_3. To the best of our knowledge, no-one has previously investigated the oxidation of organic monolayer at the air–water interface by NO_3 by in situ kinetic measurements of the surface excess.

NR experiments together with tailored kinetic modelling allowed us to determine the rate coefficients for the oxidation of OA, POA and MO monolayers to be $(2.8 \pm 0.7) \times 10^{-8}$ cm^2 molecule^{-1} s^{-1}, $(2.4 \pm 0.5) \times 10^{-8}$ cm^2 molecule^{-1} s^{-1} and $(3.3 \pm 0.6) \times 10^{-8}$ cm^2 molecule^{-1} s^{-1}, for fitted initial desorption lifetimes of NO_3 at the closely packed organic monolayers, $\tau_{d,NO3,1}$, of 8.1 ± 4.0 ns, 16 ± 4.0 ns and 8.1 ± 3.0 ns, respectively. The approximately doubled desorption lifetime found in the best fit for POA compared to OA & MO is consistent

with a more accessible double bond associated with the shorter alkyl chain of POA facilitating initial NO_3 attack at the double bond in a closely packed monolayer. The corresponding uptake coefficients for OA, POA and MO were found to be $(2.1 \pm 0.5) \times 10^{-3}$, $(1.7 \pm 0.3) \times 10^{-3}$ and $(2.1 \pm 0.4) \times 10^{-3}$. For the much slower NO_3-initiated oxidation of the saturated surfactant SA we estimated a rate coefficient of approximately $(5 \pm 1) \times 10^{-12}$ cm^2 $molecule^{-1}$ s^{-1} leading to an uptake coefficient of approximately $(5 \pm 1) \times 10^{-7}$.

Our investigations demonstrate that NO_3 will make a substantial contribution to the processing of unsaturated surfactants at the air–water interface during the night given its reactivity is ca. two orders of magnitude higher than that of O_3. Furthermore, the relative contributions of NO_3 and O_3 to the oxidative losses vary massively between structurally closely related species: NO_3 reacts ~ 384 times faster than O_3 with the most common model surfactant OA, but only ~ 58 times faster with its methyl ester MO. It is therefore required to perform a case-by-case assessment of the relative contributions of the different degradation routes for any specific surfactant. The impact of NO_3 on the fate of saturated surfactants is slightly less well quantified given the limited kinetic data, but NO_3 is very likely to be a key contributor to the loss of saturated species at night-time taking over from OH-dominated loss during the day.

The retention of the organic character at the air–water interface also differs fundamentally between the surfactant species studied. On the one hand, the fatty acids (OA and POA) form products stable at the air–water interface with yields of ~ 15–20%. On the other hand, NO_3-initiated oxidation of the oleic acid methyl ester MO rapidly removes the organic character from the surface of the aqueous droplet (≤ 3% surface-active products). The film-forming potential of reaction products will thus depend on the relative proportions of saturated and unsaturated surfactants as well as the head group properties.

The lifetime with respect to NO_3-initiated oxidation of an organic monolayer of monounsaturated molecules is about 5 to 7 minutes, while it becomes about 21 days for saturated species. Actual atmospheric residence times of unsaturated species are much longer than the lifetimes determined with respect to their reactions at the air–water interface, so it follows that they must be protected from oxidative attack *e.g.* by incorporation into a complex aerosol matrix or in mixed surface films with yet unexplored kinetic behaviour.

Acknowledgements

The authors are grateful to Prof. Ulrich Pöschl and Dr Manabu Shiraiwa for expert advice on the PRA modelling. The authors would like to thank Dr Francesco Piscitelli and Dr Ernesto Scoppola for the help during the night shifts on FIGARO. We would like to thank the Partnership for Soft Condensed Matter for access to the ellipsometer, and the ILL (Grenoble, France) for allocations of beam time on FIGARO. FS is grateful for support from the ILL and the University of Reading in the framework of the NEATNOx studentship. KR is grateful to NERC for his studentship. CP thanks NERC (grant number NE/G000883/1) for support.

References

Adams, E. & Allen, H. Palmitic Acid on Salt Subphases and in Mixed Monolayers of Cerebrosides: Application to Atmospheric Aerosol Chemistry. *Atmosphere (Basel)*. **4,** 315–336 (2013).

Allan, J. D. *et al.* Contributions from transport, solid fuel burning and cooking to primary organic aerosols in

two UK cities. *Atmos. Chem. Phys.* **10,** 647–668 (2010).

Allodi, G., FMINUIT - A binding to Minuit for Matlab, Octave & Scilab.

Angus-Smyth, A., Campbell, R.A. & Bain, C.D., Dynamic Adsorption of Weakly Interacting Polymer/Surfactant Mixtures at the Air/Water Interface. *Langmuir* **28**, 12479–12492 (2012)

Braun, L., Uhlig, M., von Klitzing, R. & Campbell, R. A. Polymers and Surfactant at Fluid Interfaces studied with Specular Neutron Reflectometry. *Adv. Colloid Interface Sci.* **247**, 130–148 (2017).

Campbell, R. A., Wacklin, H. P., Sutton, I., Cubitt, R. & Fragneto, G. FIGARO: The new horizontal neutron reflectometer at the ILL. *Eur. Phys. J. Plus* **126,** 107 (2011).

Campbell, R. A., Tummino, A., Noskov, B. A. & Varga, I. Polyelectrolyte/surfactant films spread from neutral aggregates. *Soft Matter* **12,** 5304–5312 (2016).

Ciumac, D. *et al.* Implications of lipid monolayer charge characteristics on their selective interactions with a short antimicrobial peptide. *Colloids Surfaces B Biointerfaces* **150,** 308–316 (2017).

Compernolle, S., Ceulemans, K. & Müller, J.-F. EVAPORATION: a new vapour pressure estimation methodfor organic molecules including non-additivity and intramolecular interactions. *Atmos. Chem. Phys.* **11,** 9431–9450 (2011).

Cosman, L. M., Knopf, D. A. & Bertram, A. K. N_2O_5 Reactive Uptake on Aqueous Sulfuric Acid Solutions Coated with Branched and Straight-Chain Insoluble Organic Surfactants. *J. Phys. Chem. A* **112,** 2386–2396 (2008a).

Cosman, L. M. & Bertram, A. K. Reactive Uptake of N_2O_5 on Aqueous H_2SO_4 Solutions Coated with 1-Component and 2-Component Monolayers. *J. Phys. Chem. A* **112,** 4625–4635 (2008b).

Docherty, K. S. & Ziemann, P. J. Reaction of Oleic Acid Particles with NO_3 Radicals: Products, Mechanism, and Implications for Radical-Initiated Organic Aerosol Oxidation. *J. Phys. Chem. A* **110,** 3567–3577 (2006).

Estillore, A. D., Trueblood, J. V & Grassian, V. H. Atmospheric chemistry of bioaerosols: heterogeneous and multiphase reactions with atmospheric oxidants and other trace gases. *Chem. Sci.* **7,** 6604–6616 (2016).

Fu, P. Q., Kawamura, K., Chen, J., Charrière, B. & Sempéré, R. Organic molecular composition of marine aerosols over the Arctic Ocean in summer: contributions of primary emission and secondary aerosol formation. *Biogeosciences* **10,** 653–667 (2013).

Fuzzi, S. *et al.* Critical assessment of the current state of scientific knowledge, terminology, and research needs concerning the role of organic aerosols in the atmosphere, climate, and global change. *Atmos. Chem. Phys.* **6,** 2017–2038 (2006).

Gilman, J. B., Eliason, T. L., Fast, A. & Vaida, V. Selectivity and stability of organic films at the air–acqueous interface. *J. Colloid Interface Sci.* **280,** 234–243 (2004).

Gržinic, G., Bartels-Rausch, T., Berkemeier, T., Türler, A. & Ammann, M. Viscosity controls humidity dependence of N_2O_5 uptake to citric acid aerosol. *Atmos. Chem. Phys.* **15**, 13615–13625 (2015)

Gross, S., Iannone, R., Xiao, S. & Bertram, A. K. Reactive uptake studies of NO_3 and N_2O_5 on alkenoic acid, alkanoate, and polyalcohol substrates to probe nighttime aerosol chemistry. *Phys. Chem. Chem. Phys.* **11,** 7792–7803 (2009).

Gross, S. & Bertram, A. K. Reactive Uptake of NO_3, N_2O_5, NO_2, HNO_3, and O_3 on Three Types of Polycyclic Aromatic Hydrocarbon Surfaces. *J. Phys. Chem. A* **112**, 3104–3113 (2008).

Gross, S. & Bertram, A. K. Products and kinetics of the reactions of an alkane monolayer and a terminal alkene monolayer with NO_3 radicals. *J. Geophys. Res. Atmos.* **114,** (2009).

Hearn, J. D., Lovett, A. J. & Smith, G. D. Ozonolysis of oleic acid particles: evidence for a surface reaction and secondary reactions involving Criegee intermediates. *Phys. Chem. Chem. Phys.* **7,** 501–511 (2005).

Huff Hartz, K. E., Weitkamp, E. A., Sage, A. M., Donahue, N. M. & Robinson, A. L. Laboratory measurements of the oxidation kinetics of organic aerosol mixtures using a relative rate constants approach. *J. Geophys. Res.* **112,** D04204 (2007).

Hung, H. M., Katrib, Y. & Martin, S. T. Products and mechanisms of the reaction of oleic acid with ozone and nitrate radical. *J. Phys. Chem. A* **109,** 4517–4530 (2005).

Jones, S. H. *et al.* Are organic films from atmospheric aerosol and sea water inert to oxidation by ozone at the air–water interface? *Atmos. Environ.* **161,** 274–287 (2017).

King, M. D., Thompson, K. C. & Ward, A. D. Laser Tweezers Raman Study of Optically Trapped Aerosol Droplets of Seawater and Oleic Acid Reacting with Ozone: Implications for Cloud-Droplet Properties. *J. Am. Chem. Soc.* **126,** 16710–16711 (2004).

King, M. D. *et al.* Oxidation of oleic acid at the air–water interface and its potential effects on cloud critical supersaturations. *Phys. Chem. Chem. Phys.* **11,** 7699–7707 (2009).

King, M. D., Rennie, A. R., Pfrang, C., Hughes, A. V & Thompson, K. C. Interaction of nitrogen dioxide (NO_2) with a monolayer of oleic acid at the air–water interface – A simple proxy for atmospheric aerosol. *Atmos. Environ.* **44,** 1822–1825 (2010).

Knopf, D. A., Anthony, L. M. & Bertram, A. K. Reactive Uptake of O_3 by Multicomponent and Multiphase Mixtures Containing Oleic Acid. *J. Phys. Chem. A* **109,** 5579–5589 (2005).

Knopf, D. A., Mak, J., Gross, S. & Bertram, A. K. Does atmospheric processing of saturated hydrocarbon surfaces by NO_3 lead to volatilization? *Geophys. Res. Lett.* **33,** (2006).

Knopf, D. A., Cosman, L. M., Mousavi, P., Mokamati, S. & Bertram, A. K. A Novel Flow Reactor for Studying Reactions on Liquid Surfaces Coated by Organic Monolayers: Methods, Validation, and Initial Results. *J. Phys. Chem. A* **111,** 11021–11032 (2007).

Knopf, D. A., Forrester, S. M. & Slade, J. H. Heterogeneous oxidation kinetics of organic biomass burning aerosol surrogates by O_3, NO_2, N_2O_5, and NO_3. *Phys. Chem. Chem. Phys.* **13,** 21050–21062 (2011).

Kuhne, R., Ebert, R.-U., Kleint, F., Schmidt, G. & Schuurmann, G. Group Contribution Methods to Estimate Water Solubility of Organic Chemicals. *Chemosphere* **30,** 2061–2077 (1995).

Lu, J. R., Thomas, R. K. & Penfold, J. Surfactant layers at the air/water interface: structure and composition. *Adv. Colloid Interface Sci.* **84,** 143–304 (2000).

MATLAB. *version 7.12.0 (R2011a)*. (The Math Works Inc., 2011).

Moise, T. & Rudich, Y. Uptake of Cl and Br by organic surfaces-A perspective on organic aerosols processing by tropospheric oxidants. *Geophys. Res. Lett.* **28,** 4083–4086 (2001).

Moise, T., Talukdar, R. K., Frost, G. J., Fox, R. W. & Rudich, Y. Reactive uptake of NO_3 by liquid and frozen organics. *J. Geophys. Res. Atmos.* **107,** AAC 6-1–AAC 6-9 (2002).

Mora-Diez, N. & Boyd, R. J. A Computational Study of the Kinetics of the NO_3 Hydrogen-Abstraction Reaction from a Series of Aldehydes (XCHO: X = F, Cl, H, CH_3). *J. Phys. Chem. A* **106,** 384–394 (2002).

Morris, J. W. *et al.* Kinetics of submicron oleic acid aerosols with ozone: A novel aerosol mass spectrometric technique. *Geophys. Res. Lett.* **29,** 71–74 (2002).

Narayanan, T., Wacklin, H., Konovalov, O. & Lund, R. Recent applications of synchrotron radiation and neutrons in the study of soft matter. *Crystallogr. Rev.* **23**, 160–226 (2017).

Ng, N. L. *et al.* Nitrate radicals and biogenic volatile organic compounds: oxidation, mechanisms, and organic aerosol. *Atmos. Chem. Phys.* **17,** 2103–2162 (2017).

Ots, R. *et al.* Model simulations of cooking organic aerosol (COA) over the UK using estimates of emissions based on measurements at two sites in London. *Atmos. Chem. Phys.* **16,** 13773–13789 (2016).

Pfrang, C., Shiraiwa, M. & Pöschl, U. Coupling aerosol surface and bulk chemistry with a kinetic double layer model (K2–SUB): oxidation of oleic acid by ozone. *Atmos. Chem. Phys.* **10,** 4537–4557 (2010).

Pfrang, C., Shiraiwa, M. & Pöschl, U. Chemical ageing and transformation of diffusivity in semi-solid multi-component organic aerosol particles. *Atmos. Chem. Phys.* **11,** 7343–7354 (2011).

Pfrang, C. *et al.* Ozonolysis of methyl oleate monolayers at the air–water interface: oxidation kinetics, reaction products and atmospheric implications. *Phys. Chem. Chem. Phys.* **16,** 13220–13228 (2014).

Pfrang, C., Rastogi, K., Cabrera-Martinez, E. R., Seddon, A.M., Dicko, C., Labrador, A., Plivelic, T. S., Cowieson, N. & Squires, A.M. Complex three-dimensional self-assembly in proxies for atmospheric aerosols, *Nat. Commun.* **8**, in press (2017).

Pöschl, U., Rudich, Y. & Ammann, M. Kinetic model framework for aerosol and cloud surface chemistry and gas-particle interactions - Part 1: General equations, parameters, and terminology. *Atmos. Chem. Phys.* **7,** 5989–6023 (2007).

Robinson, A. L., Donahue, N. M. & Rogge, W. F. Photochemical oxidation and changes in molecular composition of organic aerosol in the regional context. *J. Geophys. Res. Atmos.* **111** (2006).

Sebastiani, F., Campbell, R. A. & Pfrang, C. Complementarity of neutron reflectometry and ellipsometry for the study of atmospheric reactions at the air–water interface. *RSC Adv.* **5,** 107105–107111 (2015).

Seddon, A. M. *et al.* Control of Nanomaterial Self-Assembly in Ultrasonically Levitated Droplets. *J. Phys. Chem. Lett.* **7,** 1341–1345 (2016).

Seinfeld, J. H. & Pandis, S. N. *Atmospheric Chemistry and Physics: From Air Pollution to Climate Change*. (John Wiley & Sons, Inc., 2006).

Shastri, L. V & Huie, R. E. Rate constants for Hydrogen abstraction reactions of NO_3 in aqueous solution. *Int. J. Chem. Kinet.* **22,** 505–512 (1990).Shindell, D. T. *et al.* Improved Attribution of Climate Forcing to Emissions. *Science* **326** (5953), 716–718 (2009).

Shiraiwa, M., Garland, R. M. & Pöschl, U. Kinetic double-layer model of aerosol surface chemistry and gas-particle interactions (K2–SURF): Degradation of polycyclic aromatic hydrocarbons exposed to O_3, NO_2, H_2O, OH and NO_3. *Atmos. Chem. Phys.* **9,** 9571–9586 (2009).

Shiraiwa, M., Pfrang, C. & Pöschl, U. Kinetic multi-layer model of aerosol surface and bulk chemistry (KM–SUB): the influence of interfacial transport and bulk diffusion on the oxidation of oleic acid by ozone. *Atmos. Chem. Phys.* **10,** 3673–3691 (2010).

Shiraiwa, M., Ammann, M., Koop, T. & Pöschl, U. Gas uptake and chemical aging of semisolid organic aerosol particles. *Proc. Natl. Acad. Sci.* **108,** 11003–11008 (2011).

Shiraiwa, M., Pfrang, C., Koop, T. & Pöschl, U. Kinetic multi-layer model of gas-particle interactions in aerosols and clouds (KM–GAP): linking condensation, evaporation and chemical reactions of organics, oxidants and water. *Atmos. Chem. Phys.* **12,** 2777–2794 (2012a).

Shiraiwa, M., Pöschl, U. & Knopf, D. A. Multiphase Chemical Kinetics of NO_3 Radicals Reacting with Organic Aerosol Components from Biomass Burning. *Environ. Sci. Technol.* **46,** 6630–6636 (2012b).

Shiraiwa, M., Zuend, A., Bertram, A. K. & Seinfeld, J. H. Gas-particle partitioning of atmospheric aerosols: interplay of physical state, non-ideal mixing and morphology. *Phys. Chem. Chem. Phys.* **15,** 11441–11453 (2013).

Skoda, M. W. A., Thomas, B., Hagreen, M., Sebastiani, F. & Pfrang, C. Simultaneous neutron reflectometry and infrared reflection absorption spectroscopy (IRRAS) study of mixed monolayer reactions at the air–water interface. *RSC Adv.* **7,** 34208–34214 (2017).

Smith, G. D., Woods, E., DeForest, C. L., Baer, T. & Miller, R. E. Reactive Uptake of Ozone by Oleic Acid Aerosol Particles: Application of Single-Particle Mass Spectrometry to Heterogeneous Reaction Kinetics. *J. Phys. Chem. A* **106,** 8085–8095 (2002).

Sobanska, S. *et al.* Influence of stearic acid coating of the NaCl surface on the reactivity with NO_2 under humidity. *Phys. Chem. Chem. Phys.* **17,** 10963–10977 (2015).

Stevens, B. & Feingold, G. Untangling aerosol effects on clouds and precipitation in a buffered system. *Nature* **461,** 607–613 (2009).

Stocker, T. F. *et al.* Contribution of Working Group I to the Fifth Assessment Report of the Intergovernmental Panel on Climate Change. in *'Climate Change 2013: The Physical Science Basis'* (Cambridge University Press, 2013). doi:10.1017/CBO9781107415324

Tervahattu, H., Juhanoja, J. & Kupiainen, K. Identification of an organic coating on marine aerosol particles by TOF-SIMS. *J. Geophys. Res. Atmos.* **107,** ACH 18-1–ACH 18-7 (2002a).

Tervahattu, H. *et al.* New evidence of an organic layer on marine aerosols. *J. Geophys. Res. Atmos.* **107,** AAC 1-1–AAC 1-8 (2002b).

Thompson, K. C. *et al.*, Reaction of a phospholipid monolayer with gas-phase ozone at the air-water interface: measurement of surface excess and surface pressure in real time. *Langmuir*, **26**, 17295–303 (2010).

Thompson, K. C. *et al.* Degradation and Rearrangement of a Lung Surfactant Lipid at the Air–Water Interface during Exposure to the Pollutant Gas Ozone. *Langmuir* **29,** 4594–4602 (2013).

Vesna, O. *et al.* Changes of fatty acid aerosol hygroscopicity induced by ozonolysis under humid conditions. *Atmos. Chem. Phys.* **8,** 4683–4690 (2008).

Virtanen, A. *et al.* An amorphous solid state of biogenic secondary organic aerosol particles. *Nature* **467,** 824–827 (2010).

Wadia, Y., Tobias, D. J., Stafford, R. & Finlayson-Pitts, B. J. Real-Time Monitoring of the Kinetics and Gas-

Phase Products of the Reaction of Ozone with an Unsaturated Phospholipid at the Air–Water Interface. *Langmuir* **16,** 9321–9330 (2000).

Wang, Y., Cannon, F. S., Salama, M., Fonseca, D. A. & Giese, S. Characterization of Pyrolysis Products from a Biodiesel Phenolic Urethane Binder. *Environ. Sci. Technol.* **43,** 1559–1564 (2009).

Wayne, R. P. *et al.* The nitrate radical: Physics, chemistry, and the atmosphere. *Atmos. Environ. Part A. Gen. Top.* **25,** 1–203 (1991).

Xiao, S. & Bertram, A. K. Reactive uptake kinetics of NO_3 on multicomponent and multiphase organic mixtures containing unsaturated and saturated organics. *Phys. Chem. Chem. Phys.* **13,** 6628–6636 (2011).

Zahardis, J. & Petrucci, G. A. The oleic acid-ozone heterogeneous reaction system: products, kinetics, secondary chemistry, and atmospheric implications of a model system – a review. *Atmos. Chem. Phys.* **7,** 1237–1274 (2007).

Zhang, P. *et al.* Effects of Humidity and $[NO_3]/[N_2O_5]$ Ratio on the Heterogeneous Reaction of Fluoranthene and Pyrene with $N_2O_5/NO_3/NO_2$. *Environ. Sci. Technol.* **48**, 13130−13137 (2014a).

Zhang, Y. *et al.* Gas-surface reactions of nitrate radicals with vinyl-terminated self-assembled monolayers. *Phys. Chem. Chem. Phys.* **16,** 16659–16670 (2014b).

Zhao, Z., Husainy, S., Stoudemayer, C. T. & Smith, G. D. Reactive uptake of NO_3 radicals by unsaturated fatty acid particles. *Phys. Chem. Chem. Phys.* **13,** 17809–17817 (2011).

Ziemann, P. J. Aerosol products, mechanisms, and kinetics of heterogeneous reactions of ozone with oleic acid in pure and mixed particles. *Faraday Discuss.* **130,** 469–490 (2005).